

STEAM REFORMING OF ETHANOL FOR HYDROGEN PRODUCTION
USING CU-MCM41 AND NI-MCM41 TYPE MESOPOROUS CATALYTIC
MATERIALS

A THESIS SUBMITTED TO
THE GRADUATE SCHOOL OF NATURAL AND APPLIED SCIENCES
OF
MIDDLE EAST TECHNICAL UNIVERSITY

BY

EKİN ÖZDOĞAN

IN PARTIAL FULFILLMENT OF THE REQUIREMENTS
FOR
THE DEGREE OF MASTER OF SCIENCE
IN
CHEMICAL ENGINEERING

AUGUST 2007

Approval of the thesis:

**“STEAM REFORMING OF ETHANOL FOR HYDROGEN PRODUCTION
USING CU-MCM41 AND NI-MCM41 TYPE MESOPOROUS CATALYTIC
MATERIALS”**

submitted by **EKİN ÖZDOĞAN** in partial fulfillment of the requirements for the degree of Master of Science in **Chemical Engineering Department, Middle East Technical University** by,

Prof. Dr. Canan Özgen _____
Dean, Graduate School of **Natural and Applied Sciences**

Prof. Dr. Nurcan Baç _____
Head of Department, **Chemical Engineering**

Prof. Dr. Timur Doğu _____
Supervisor, **Chemical Engineering, METU**

Examining Committee Members:

Prof. Dr. H. Tunçer Özdamar _____
Chemical Engineering Dept., Ankara University

Prof. Dr. Timur Doğu _____
Chemical Engineering Dept., METU

Assoc. Prof. Dr. Naime A. Sezgi _____
Chemical Engineering Dept., METU

Assoc. Prof. Dr. Göknur Bayram _____
Chemical Engineering Dept., METU

Assist. Prof. Dr. Meltem Doğan _____
Chemical Engineering Dept., Gazi University

Date:

16.08.2007

I hereby declare that all information in this document has been obtained and presented in accordance with academic rules and ethical conduct. I also declare that, as required by these rules and conduct, I have fully cited and referenced all material and results that are not original to this work.

Name, Last name: Ekin ÖZDOĞAN

Signature

ABSTRACT

STEAM REFORMING OF ETHANOL FOR HYDROGEN PRODUCTION USING CU-MCM41 AND NI-MCM41 TYPE MESOPOROUS CATALYTIC MATERIALS

Özdoğan, Ekin

M.Sc., Department of Chemical Engineering

Supervisor: Prof. Dr. Timur DOĞU

August, 2007, 106 pages

The world's being alerted to the global warming danger and the depletion of fossil fuel resources, has increased the importance of the clean and renewable hydrogen energy. Bioethanol has high potential to be used as a resource of hydrogen since it is a non-petroleum feedstock and it is able to produce hydrogen rich mixture by steam reforming reactions. Discovery of mesoporous MCM-41 type high surface area silicate-structured materials with narrow pore size distributions (20-100 Å) and high surface areas (up to 1500 m²/g) opened a new avenue in catalysis research. Catalytic activity of such mesoporous materials are enhanced by the incorporation of active metals or metal oxides into their structure. Nickel and copper are among the most active metals to be used in steam reforming of ethanol to produce hydrogen.

In this study, copper and nickel incorporated MCM-41 type catalytic materials were tested in the steam reforming of ethanol. Two Ni-MCM-41 samples having different Ni/Si ratios were prepared by high temperature direct synthesis

method and two Cu-MCM-41 samples having same Cu/Si ratios were synthesized by two different methods namely, high temperature direct synthesis method and impregnation method. The synthesized materials characterized by XRD, EDS, SEM, N₂ physisorption and TPR techniques.

XRD results showed that Ni-MCM-41 and Cu-MCM-41 catalysts had typical MCM-41 structure. The d_{100} and lattice parameter values of Ni-HT (I) (Ni-MCM-41 sample having 0.036 Ni/Si atomic ratio) was obtained as 3.96 and 4.57 nm., respectively. In addition Ni-HT (I) was found to have a surface area of 860.5 m²/g and 2.7 nm pore diameter. The d_{100} and lattice parameter values for a typical Cu-MCM-41 prepared by impregnation method having Cu/Si atomic ratio of 0.19 were obtained as 3.6 and 4.2 nm., respectively. This sample also has a 631 m²/g surface area and 2.5 nm pore diameter.

Steam reforming of ethanol was investigated in the vapor phase by using Ni-MCM-41 and Cu-MCM-41 catalysts between 300°C and 550°C. Results proved that Ni incorporated MCM-41 type catalytic materials were highly active in hydrogen production by steam reforming of ethanol and actualized almost complete ethanol conversion for Ni-MCM-41 having Ni/Si atomic ratio of 0.15 over 500°C . The side products obtained during reforming are methane and formaldehyde. Although the Cu-MCM-41 samples were not as active as Ni-MCM-41, it was observed that Cu-MCM-41 catalyst synthesized by the impregnation method showed an ethanol conversion of 0.83. However, the main product was ethylene with the copper incorporated catalysts. Effects of space time, the operating conditions (reaction temperature), metal/Si ratio of the catalyst and the preparation method on the product distributions were also investigated and best reaction conditions were searched.

Keywords: Ni-MCM-41, Cu-MCM-41, Steam Reforming, Ethanol, Hydrogen

ÖZ

CU-MCM41 VE Ni-MCM41 TİPİ MEZOGÖZENEKLİ KATALİTİK MALZEMELER KULLANILARAK BUHAR REFORMİNG TEPKİMESİYLE ETANOLDEN HİDROJEN ÜRETİMİ

Özdoğan, Ekin

Yüksek Lisans, Kimya Mühendisliği

Tez Danışmanı: Prof. Dr. Timur DOĞU

Ağustos, 2007, 106 sayfa

Dünyanın küresel ısınma tehlikesine karşı alarma geçmesi ve fosil yakıt kaynaklarının tükenmesi temiz ve yenilenebilir hidrojen enerjisinin önemini arttırmıştır. Petrol kökenli olmayan bir hammadde oluşu ve buharlı reforming tepkimeleriyle hidrojen zengin çözeltiler üretmesi nedeniyle, biyoetanol hidrojen kaynağı olarak kullanılmak için yüksek bir potansiyele sahiptir. MCM-41 tipi yüksek yüzey alanlı silika yapılı, dar gözenek boyutu dağılımlı (20-100 Å) ve yüksek yüzey alanlı (1500 m²/g e kadar) mezogözenekli malzemelerin keşfi katalizör araştırmalarında yeni bir yol açmıştır. Bu tür mezogözenekli malzemelerin katalitik aktiviteleri yapılarına aktif metal veya metal oksit eklenmesiyle artırılır. Nikel ve bakır, etanolün buhar reforming ile hidrojen üretiminde en çok kullanılan aktif metaller arasındadır.

Bu çalışmada, bakır ve nikel eklenmiş MCM-41 tipi katalizörler etanolün buhar reforming ile test edilmiştir. İki adet farklı Ni/Si oranına sahip Ni-MCM-41, yüksek sıcaklıkta doğrudan ekleme yöntemiyle ve iki adet aynı Cu/Si oranına sahip Cu-MCM-41 de iki farklı yöntemle , yani yüksek sıcaklıkta doğrudan ekleme yöntemi ve sonradan ekleme yöntemi ile hazırlanmıştır. Sentezlenen malzemeler XRD, EDS, SEM, N₂ fiziksel adsorplanması ve TPR teknikleriyle karakterize edilmiştir.

XRD sonuçları, Ni-MCM-41 ve Cu-MCM-41' in tipik MCM-41 yapısına sahip olduklarını göstermiştir. Ni- HT (I)'in (0.036 Ni/Si atom oranına sahip Ni-MCM-41 numunesi) d₁₀₀ ve kafes parametresi sırasıyla 3.96 ve 4.57 nm olarak elde edilmiştir. Ayrıca, Ni-HT (I) 860.5 m²/g yüzey alanına ve 2.7 nm gözenek çapına sahiptir. Cu/Si atom oranı 0.19 olan ve sonradan ekleme yöntemiyle hazırlanan tipik bir Cu-MCM-41'in d₁₀₀ ve kafes parametre değerleri sırasıyla 3.6 ve 4.2 nm dir. Bu numune aynı zamanda 631 m²/g yüzey alanına ve 2.5 nm gözenek çapına sahiptir.

Etanolun buhar reforming'i buhar fazında, 300°C ila 550°C arasında Ni-MCM-41 ve Cu-MCM-41 kullanılarak incelenmiştir. Sonuçlar, Ni eklenmiş MCM-41 tipi katalitik malzemelerin etanolden buhar reforming ile hidrojen üretiminde aktif olduğunu ve 0.15 Ni/Si atom oranına sahip Ni-MCM-41 in 500°C nin üzerinde etanolün yaklaşık tümünün dönüşümünü gerçekleştirdiğini kanıtlamıştır. Reforming sırasında elde edilen yan ürünler metan ve formaldehittir. Ni-MCM-41 kadar aktif olmamasına rağmen, sonradan ekleme yöntemiyle hazırlanan Cu-MCM-41 in etanol dönüşüm değerinin 0.83 olduğu gözlenmiştir. Ancak, bakır eklenmiş katalizörlerin oluşturduğu temel ürün etilen olmuştur. Alan zamanının, çalışma koşullarının (reaksiyon sıcaklığı gibi), katalizörün metal/Si oranının ve hazırlama metodunun ürün dağılımına olan etkisi de incelenmiş ve en iyi reaksiyon koşulları araştırılmıştır.

Anahtar Sözcükler: Ni-MCM-41, Cu-MCM-41, Buhar Reforming, Etanol, Hidrojen

To Umut, Nilufer and Seref

ACKNOWLEDGEMENTS

First and foremost acknowledgements go to my supervisor Prof. Dr. Timur Dogu for his support and guidance throughout my studies. His contributions to my engineering career and encouragements motivated and inspired me. Without his orientation, this work would not be possible. I would also like to present my gratefulness to Prof. Dr. Gulsen Dogu for her valuable support and precious feedback on my thesis topic.

I would like to thank my lab partners, Canan Sener, Dilek Varisli, Zeynep Obali. It was very special to work with friends like you. My valuable friends Kubra Kamisoglu, Sezin Akbay and Hulya Erdener, six years were not enough at this department with you. Your patience and friendship to me was too valuable for me. Sumeyra, my sister, my best friend, thanks for being always there for me as you are now.

Finally, my all, my parents Seref and Nilufer and my brother Umut without you it was not only hard to achieve these studies but also impossible to be such a happy person. Seref and Nilufer, you were more than parents for me and will be always with me (I am sure you will be :)). Umut, I owe my success to you and I am very lucky that I have a brother like you. I love you my dears...

I am grateful to all my friends who helped me to put this work together.

TABLE OF CONTENTS

ABSTRACT	iv
ÖZ	vi
DEDICATION	viii
ACKNOWLEDGEMENTS	ix
TABLE OF CONTENTS	x
LIST OF TABLES	xiii
LIST OF FIGURES	xiv
NOMENCLATURE	xvi
CHAPTER	
1- INTRODUCTION.....	1
2- STEAM REFORMING OF ETHANOL FOR HYDROGEN PRODUCTION.....	3
1. Steam Reforming Reaction of Ethanol.....	4
2. Thermodynamics of the Steam Reforming of Ethanol.....	6
3. Catalysts Used For Steam Reforming of Ethanol.....	7
i. Oxide Catalysts.....	7
ii. Oxide supported Metal Catalysts.....	7
iii. Cu and Ni based Catalysts.....	9
3- M41S MESOPOROUS MATERIALS.....	13
1. Mesoporous Materials.....	13
2. M41S Family.....	14

i.	MCM-41.....	15
ii.	MCM-48.....	17
iii.	MCM-50.....	18
3.	Characterization of Mesoporous material MCM-41.....	19
i.	X-Ray Diffraction.....	19
ii.	N ₂ Physisorption.....	19
iii.	Scanning Electron Microscopy and Electron Dispersive Spectroscopy.....	19
4.	Studies from Literature about Cu-MCM-41 and Ni-MCM-41 Type Catalytic Materials.....	20
5.	Objectives of the Study.....	21
4-	EXPERIMENTAL.....	23
1.	Catalyst Preparation.....	23
i.	Chemicals.....	23
ii.	Preparation of Ni-MCM-41 by High Temperature Direct Synthesis Method.....	24
iii.	Preparation of Cu-MCM-41 by High Temperature Direct Synthesis Method	25
iv.	Preparation of Cu-MCM-41 by Impregnation Method	25
2.	Catalyst Characterization.....	26
i.	X-Ray Diffraction (XRD)	26
ii.	Energy Dispersive Spectroscopy (EDS)	26
iii.	Nitrogen Physisorption.....	26
iv.	Scanning Electron Microscopy (SEM)	27
v.	Temperature Programmed Reduction (TPR).....	27
3.	Steam Reforming Reaction Set-up.....	27
5-	RESULTS AND DISCUSSIONS.....	32
1.	Characterization of Catalysts	32
i.	XRD.....	32
ii.	EDS and SEM.....	36
iii.	N ₂ Physisorption.....	39

iv.	TPR.....	42
2.	Steam Reforming of Ethanol via Ni-MCM-41 and Cu-MCM-41 Catalysts.....	44
i.	Catalytic Activity of Nickel Based MCM-41 type catalysts.....	45
a.	Conversion of Ethanol.....	46
b.	Yield of hydrogen.....	47
c.	Selectivity of Side Products.....	49
ii.	Catalytic Activity of Copper Based MCM-41 type catalysts.....	55
a.	Conversion of Ethanol.....	56
b.	Yield of hydrogen.....	57
c.	Selectivity of Side Products.....	58
6-	CONCLUSIONS & RECOMMENDATIONS.....	63
7-	REFERENCES.....	66
8-	APPENDIX A.....	75
1.	EDS.....	75
2.	SEM.....	77
9-	APPENDIX B.....	78
1.	RAW REACTION DATA.....	78
2.	CALIBRATION FACTORS (BETA FACTORS) OF THE SPECIES.....	99
3.	SAMPLE CALCULATIONS OF THE REACTION PARAMETERS.....	101
4.	CALCULATED REACTION PARAMETERS.....	104

LIST OF TABLES

Table 1. The programme information of the Gas Chromatograph.....	28
Table 2. The set points of the parameters of GC.....	29
Table 3. d_{100} and a values for the catalysts.....	35
Table 4. EDS analysis of the Ni-HT (I), Ni-HT (II), Cu-HT (I) and Cu-Imp (II).....	37
Table 5. Pore Diameter, Pore Wall Thickness and BET Surface Area Data of the Synthesized Catalysts.....	41
Table 6. The Summary of the Characterization Results.....	43
Table 7. The summary of reaction parameters of Ni-HT (I), Ni-HT (II), Cu-HT (I) and Cu-Imp (II).....	44
Table 8. The variation of Formaldehyde yield with temperature.....	52
Table 9. Ethylene selectivity data for Ni-HT (I)aa, Ni-HT (I)b and Ni-HT (II).....	55
Table 10. The change of selectivity of CO with temperature.....	61
Table 11. The variation of selectivity of methane with temperature.....	61
Table 12. The variation of selectivity of CO ₂ with temperature.....	62
Table 13. Raw Data Of Ni-HT (I)a.....	78
Table 14. Raw Data Of Ni-HT (I)b.....	82
Table 15. Raw Data Of Ni-HT (II).....	86
Table 16. Raw Data Of Cu-HT (I).....	91
Table 17. Raw Data Of Cu-Imp (II).....	95
Table 18 The calibration values for elements using CTR column.....	99
Table 19 The calibration values for elements using Porapak S column.....	100
Table 20. Raw Data of Ni-HT (II) at 550°C.....	101
Table 21. Calculated Reaction Parameters.....	104

LIST OF FIGURES

Figure .1. Possible reaction mechanisms for steam reforming of ethanol.....	5
Figure 2. Phase sequence of water- surfactant binary system.....	14
Figure 3.(a) The front view of the MCM-41 uni-directional channels, (b) TEM image of the MCM-41	15
Figure 4. Schematic model of liquid crystal templating mechanism via two possible pathways	16
Figure 5. (a) The proposed 3D view of MCM-48 structure , (b) The schematic representation of proposed model of MCM-48	17
Figure 6. The schematic representation of MCM-50	18
Figure 7. Schematic representation of (a) high temperature direct synthesis method, (b) impregnation method.....	30
Figure 8. The real image of reaction set-up.....	31
Figure 9. Schematic representation of the reaction set-up.....	31
Figure 10. The schematic representation of Bragg's Law	33
Figure 11. XRD pattern of Ni-HT (I) catalyst.....	34
Figure 12. XRD pattern of Ni-HT (II) catalyst.....	34
Figure 13. XRD pattern of Cu-HT (I) catalyst.....	34
Figure 14. XRD pattern of Cu-Imp (II) catalyst.....	34
Figure 15. XRD pattern of Ni-HT (I) catalyst (wide angle range)	36
Figure 16. XRD pattern of Ni-HT (II) catalyst (wide angle range)	36
Figure 17. SEM image of Ni-HT (I).....	38
Figure 18. SEM image of Ni-HT (II).....	38
Figure 19. SEM image of Cu-HT (I).....	38
Figure 20. SEM image of Cu-Imp (II).....	38
Figure 21. Isotherm of Ni-HT (I).....	39
Figure 22. Isotherm of Ni-HT (II).....	39

Figure 23. Isotherm of Cu-HT (I).....	39
Figure 24. Isotherm of Cu-Imp (II).....	39
Figure 25. Pore size distribution of Ni-HT (I).....	40
Figure 26. Pore size distribution of Ni-HT(II).....	40
Figure 27. Pore size distribution of Cu-HT (I).....	40
Figure 28 Pore size distribution of Cu Imp (II).....	40
Figure 29. Temperature Programmed Reduction Profile of Ni-HT (I).....	42
Figure 30. Variation of conversion of ethanol with temperature.....	46
Figure 31. Variation of hydrogen yield with temperature.....	48
Figure 32. The variation of selectivity of CO with temperature.....	49
Figure 33 The variation of CH ₄ selectivity with temperature.....	50
Figure 34 The variation of formaldehyde selectivity with temperature.....	51
Figure 35. The selectivity of CO ₂ (A) for Ni-HT (I)a and Ni-HT (I)b (B) for Ni-HT (II).....	54
Figure 36. Variation of conversion of ethanol with temperature.....	56
Figure 37. Variation of hydrogen yield with temperature.....	57
Figure 38. The variation of selectivity of ethylene with temperature.....	58
Figure 39. The variation of ethylene yield with temperature.....	59
Figure 40. The change of selectivity of formaldehyde with temperature.....	60
Figure 41. EDS of Ni-HT (I).....	75
Figure 42. EDS of Ni-HT (II).....	75
Figure 43. EDS of Cu-HT (I).....	76
Figure 44. EDS of Cu-Imp (II)	76
Figure 45. SEM image of Ni-HT (I)	77
Figure 46. SEM image of Ni-HT (I).....	77
Figure 47. SEM image of Cu-HT (I).....	77
Figure 48. SEM image of Cu-Imp (II)	77

NOMENCLATURE

IUPAC: International Union of Pure and Applied Chemistry

MCM: Mobil Composition Matter

X_A : Conversion of A

x_A : Fraction of A

Y_A : Yield of A

S_A : Selectivity of A

EtOH: Ethanol

XRD: X-Ray Diffraction

EDS: Energy Dispersive Spectroscopy

SEM: Scanning Electron Microscopy

TPR: Temperature Programmed Reduction

TEM: Transmission Electron Microscopy

CHAPTER 1

INTRODUCTION

The interest in hydrogen as an alternative energy has increased due to the environmental aspects. Although there are transportation and storage problems of hydrogen, on board reforming of hydrocarbons especially alcohols makes this energy option attractive. Among alcohols, ethanol is low in toxicity, easy to store and transport, renewable and gives hydrogen rich mixture when it decomposes. For this reason many researchers studied steam reforming of ethanol with many different kinds of materials [15], [16], [20].

MCM-41 type mesoporous materials, member of M41S family, were discovered by Mobil researchers in 1992. These mesoporous materials having uniform channels ranging from 1.5 to 10 nm also have high surface area values higher than 800 m²/g and each of the M41S family members has different structures. These materials are fundamentally different from zeolites by the fact that the pore walls are amorphous. When metal integrated onto this material, it shows higher activities to various reactions. Ni and Cu are two popular metals used incorporated on catalysts used for steam reforming.

In this study, Ni-MCM-41 and Cu-MCM-41 catalysts were synthesized, characterized and used for the steam reforming of ethanol to produce hydrogen. The effects of reaction temperature, space time, metal/Si ratio in the catalysts and the synthesis method were observed.

In Chapter 2, the steam reforming reaction of ethanol, the importance of hydrogen and the reason of choosing ethanol as a feedstock were defined and

detailed information was given. Moreover, the studies performed in the literature about steam reforming of ethanol were mentioned.

In Chapter 3, M41S family and the family members; MCM-41, MCM-48 and MCM-50 were introduced. A literature survey about the performance of Cu and Ni integrated MCM-41 type materials were also given in this chapter.

Chapter 4 mainly included the experimental part of the study. In this chapter, the synthesis methods were explained and illustrated by figures. Following this chapter, in Chapter 5 the results of the experiments held during the study were given. The interpretation of the experimental data was also performed in this chapter. Finally, all the work done in the scope of this study, final remarks and suggestions were given in Conclusions and Recommendations part.

CHAPTER 2

STEAM REFORMING OF ETHANOL FOR HYDROGEN PRODUCTION

Today, major energy need is supplied by natural gas and petroleum, refined into gasoline and diesel. The fact is that while the combustion of these fossil based fuels pollutes the world by the emission of greenhouse gases, the resources of those deplete day by day. In this regard, the world has started to alarm of “global warming” problem and the need on the clean and renewable energy has become inevitable.

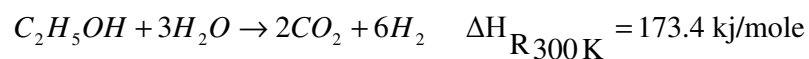
Hydrogen being abundantly available in the universe in combined form, burning cleanly and having the highest energy content per unit weight (120 kJ/g) compared to the any other known fuels e.g gasoline 46.9 kJ/g [1], comes forward among the energy solutions for the future with its advantageous properties [2].

Besides its advantages, the storage and the transportation of hydrogen are challenging problems. Hydrogen is the lightest element with the atomic weight of 1.0 and it has a density of 0.07 g/cm^3 whereas gasoline has a density of 0.75 g/cm^3 . So by considering the density and energy content of the two, hydrogen needs about four times the volume needed for gasoline for a given amount of energy [3]. In liquid form, hydrogen can only be stored under extreme frigid temperatures. These options are not practical for everyday use [4].

The storage and the transportation drawbacks can be handled by the implementation of the fuel cells by hydrocarbon processing which is the steam reforming of liquid fuels. This supplies easiness for the storage of the lightweight hydrogen and also gives opportunity for the “on board” reforming of fuels containing compounds of hydrogen [5]. Hydrogen can be produced from methane, natural gas, liquefied petroleum gas, propane, gasoline, biomass-derived liquid fuels like alcohols. Among all these alternatives, alcohols outweighs by easily decomposing into hydrogen rich mixture in the presence of water. Methanol reforming was studied by many researchers and Toyota [6] exhibited fuel cell electric vehicle working with methanol in 1997. Following this, Daimler- Benz AG cooperating with Ballard [7], also introduced the prototype of fuel cell vehicle working with methanol. On the contrary Klouz et al. [8] pointed that methanol is highly toxic and obtained from nonrenewable fossil fuels (mostly natural gas). Unlike methanol, ethanol is low in toxicity, obtained renewably from the fermentation of starch or sugar and also from low-cost vegetation, such as crop and sugar beat wastes. For this reason, it does not release greenhouse gases. In addition, it is easy to store and transport and free from catalyst poisons such as sulfur [9].

2.1. Steam Reforming Reaction of Ethanol

Overall Steam Reforming reaction of ethanol is as follows [10];



The above reaction may consist of different reaction paths depending on the catalyst used as shown in the Fig. 1.

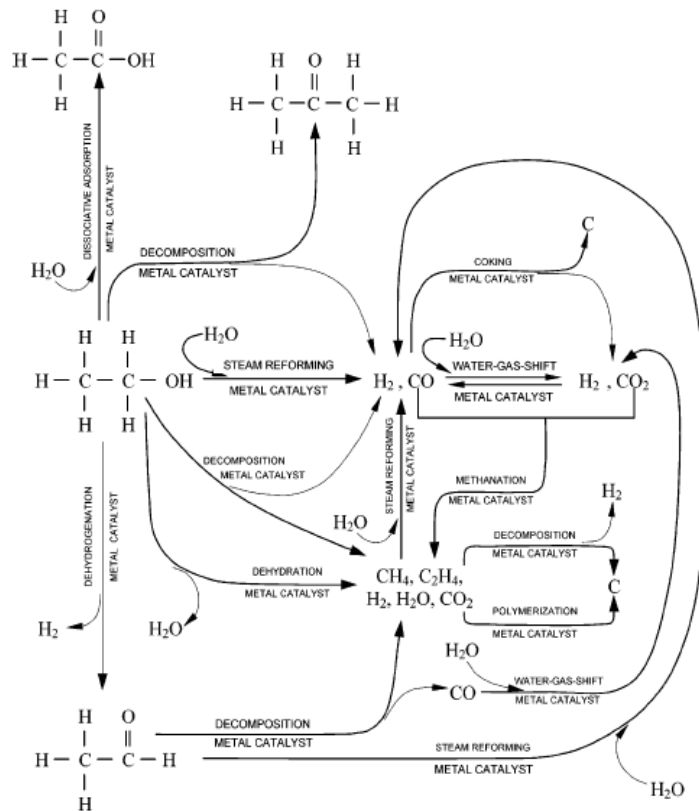
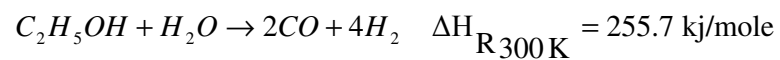


Figure 1. Possible reaction mechanisms for steam reforming of ethanol [10]

However the overall reaction can be divided mainly two different reaction steps;

- Steam Reforming Step;



- Water Gas Shift Step



Possible side products were reported as acetaldehyde, ethylene, methane and acetone. There are many studies dealt with both of the reaction steps, but for this study, only the steam reforming step was focused and introduced.

2.2. Thermodynamics of the Steam Reforming of Ethanol

Thermodynamic analysis of the reaction was performed by many researchers such as Garcia et al. [11], Vasudeva et al. [12], Fishtik et al. [13] and Ionnides [14]. Garcia et al. [11], studied the thermodynamic equilibrium of ethanol reforming reaction for the pressure 1–9 atm, temperature 400–800 K and water to ethanol feed ratio 0:1–10:1 ranges. They concluded that the optimum condition for this reaction occurs at $T > 650$ K, atmospheric pressure and water in excess in the feed. By this means, undesired methane formation is minimized and carbon formation is thermodynamically inhibited. Depending on this study, another thermodynamic study was performed by Vasudeva et al. [12] and the thermodynamic feasibility of the ethanol reforming reaction was reexamined.

Fishtik et al. [13], performed thermodynamic analysis of the reaction in terms of response reactions and concluded that at or above 700-800 K and high water/ethanol ratios, the reforming of ethanol reaction predominates and the undesired product formation can be prevented.

Another thermodynamic approach came from Ionnides [14]. His analysis were carried out with respect to solid polymer fuel cell applications and introduced that water to ethanol feed ratio should not be higher than the stoichiometry for optimum reforming reactions. The common outcome of these four studies mentioned above, was that the steam reforming of ethanol to produce hydrogen is thermodynamically feasible.

2.3. Catalysts Used For Steam Reforming of Ethanol

The complete conversion of ethanol and high hydrogen selectivity and yield are important factors affecting the process economy. At this point, catalyst plays significant role in resulting reactions since each catalyst induces different reaction paths. So the selection of the suitable catalyst is very crucial.

2.3.i. Oxide Catalysts

Llorca et al. [15] used different oxide catalysts (e.g. MgO, γ -Al₂O₃, SiO₂, ZnO, etc.) and decided that ZnO gives highly effective production of hydrogen without CO. CO is a poison for the Pt, Pd etc. catalysts present in the fuel cells. So it is important to achieve high conversion of water gas shift reaction and to decrease the CO content of the gas stream obtained in the reformer to very low levels. 5.1 moles of hydrogen is formed per mole of reacted ethanol at 723 K. The main reactions observed were the decomposition of ethanol to acetone, the reforming of ethanol and water gas shift reaction. The reaction results of the other oxides showed that negligible steam-reforming of ethanol was observed over MgO and γ -Al₂O₃. Over γ -Al₂O₃ (acidic catalyst) only the dehydration of ethanol to ethylene was observed and over MgO (basic catalyst) high selectivity to acetaldehyde was obtained through dehydrogenation of ethanol. Among all, the performance of ZnO in the steam-reforming of ethanol could be a consequence of its basic and redox characteristics.

2.3.ii. Oxide supported Metal Catalysts

- *Co Oxides Catalysts*

In 1997, Haga et al. [16] reported Co/Al₂O₃ as a promising catalyst among Co/SiO₂, Co/MgO, Co/ZrO₂ and Co/C catalysts. In addition, Batista et al. [17] supported the same idea by working with Co/Al₂O₃, Co/SiO₂, and

Co/MgO. The reason is that depending on the catalyst preparation method, the catalyst is able to convert 100% of the ethanol with 70% hydrogen selectivity. However Llorca et al. [18] showed that the amount of hydrogen produced by Co/Al₂O₃ is small when it is compared with the amount of CH₄ and C₂ compounds produced during reaction and carbon deposition occurred.

- *Rh, Pt, Pd and Ru Oxides Catalysts*

Some researchers focused on the rhodium supported on oxide catalysts. Aupretre et al. [19] investigated Rh/Al₂O₃ catalyst and concluded that this catalyst showed higher activity in steam reforming reaction than Pt, Pd, Ru, Cu, Zn and Fe metals supported on alumina catalysts. However from the study of Cavallaro [20], it was evident that rhodium loading influenced catalyst performance very much. At lower rhodium loading (0.5 wt %), this catalyst easily deactivates and produces CH₄. He also suggested a reforming reaction mechanism for this catalyst. This mechanism composed of firstly the dehydration reaction giving C₂H₄ from ethanol or dehydrogenation giving acetaldehyde, secondly decarbonylation of C₂H₄O giving CH₄ and CO and finally steam reforming of CH₄ and the shift reaction of CO. Freni [21] used again Rh/Al₂O₃ but this time with higher Rh loading (5 wt %) and they experienced 100 % conversion of ethanol at 923 K and 0.16 MPa with water to ethanol molar feed ratio of 8.4:1. Consequently further studies done by Cavallaro et al. [22], on Rh/Al₂O₃, showed that 5 wt % rhodium catalysts showed no coke formation.

Liguras et al., [23] studied steam reforming of ethanol by Rh, Ru, Pt, and Pd with the Al₂O₃, MgO, and TiO₂ supports. They concluded that for low-loaded catalysts, Rh is significantly more active and selective toward hydrogen formation compared to Ru, Pt and Pd, which show a similar behavior. They also reported that the catalytic performance of Rh and Ru increased with increasing metal loading and the catalytic activity and selectivity of high-loaded Ru catalysts were comparable to that of Rh. In addition to that, with the

5 wt % Ru/Al₂O₃ catalyst, complete conversion of ethanol was achieved and 95 % selectivity toward hydrogen was obtained with the methane formation.

Casanova et al. [24], used ZnO and SiO₂ supported palladium catalysts in the ethanol steam-reforming and oxidative ethanol steam-reforming reactions in the temperature range of 548–723 K. They found out that on silica-supported Pd catalyst, ethanol decomposes into H₂, CO and CH₄ in both steam-reforming whereas ZnO supported catalysts containing the PdZn phase exhibit a better catalytic performance for hydrogen production through dehydrogenation of ethanol into acetaldehyde and ulterior reforming.

It can be understood from the studies given above that Rh is superior in activity among noble metals for hydrogen production. At high temperature and high catalyst loading, however, Ru competes with Rh.

2.3.iii. Cu and Ni based Catalysts

As a low-cost metal Nickel, is widely used in industry. When ethanol reforming is considered Ni works well as it favors C-C bond rupture. [25] Earlier studies focused on the Cu added Ni based catalysts for steam reforming of ethanol.

Marino and his co-workers performed series of studies for ethanol reforming by using Ni-Cu based catalysts. The first one of these studies [26] includes the usage of Cu/Ni/K/γ-Al₂O₃ catalyst in the ethanol reforming. They concluded that this catalyst show acceptable activity, stability and selectivity of hydrogen at 300°C and 1 atm pressure. Moreover, copper was the active agent, nickel promoted the C-C bond rupture and increased the hydrogen selectivity and potassium neutralized the acidic sites of γ alumina improving the general performance of the catalyst. Three years later, more specialized study was published by Marino et al. [27]. In this study they worked with the same catalyst but they dealt this time with the effect of nickel more extensively. It was understood that Ni addition to Cu/Ni/K/γ-Al₂O₃ catalysts favors ethanol gasification, increases the gas yield and reduces acetaldehyde and acetic acid production. The presence of Ni slightly increases the hydrogen production

through a mild increase of ethanol conversion since it favors the segregation of Cu^{+2} ions to the catalytic surface. Final study done by Marino et al., [28] proposed ethanol gasification mechanism by using $\text{Cu/Ni/K}/\gamma\text{-Al}_2\text{O}_3$. A mechanism that involves differentiated copper and nickel sites is suggested. The experimental results obtained in absence of water were explained from this mechanism.

The studies done by nickel metal integrated on $\gamma\text{-Al}_2\text{O}_3$ for ethanol steam reforming reactions continued with Verykios et al. [29] with the usage of $\text{La}_2\text{O}_3/\gamma\text{-Al}_2\text{O}_3$ and Ni catalysts supported on $\gamma\text{-Al}_2\text{O}_3$ and La_2O_3 . They found out that Al_2O_3 promotes dehydration and cracking while La_2O_3 primarily promotes dehydrogenation and cracking. While experiencing carbon deposition for all their systems, they also concluded that the presence of Ni increases the reforming of ethanol and acetaldehyde as well as the water–gas shift and methanation reactions. Fierro et al., [30] added one more study to the Ni supported with Al_2O_3 subject. They studied reforming of ethanol over two different Ni (11 and 20 wt %)/ Al_2O_3 catalysts and five bimetallic catalysts that were Ni (approximately 20 wt %) based catalysts doped with Cr (0.65 wt %), Fe (0.6 wt %), Zn (0.7 wt %) or Cu (0.6 and 3.1 wt %) supported on Al_2O_3 . Finally they pointed to the fact that the order in H_2 production was Ni–Zn > Ni–Fe > Ni–Cr > Ni > Ni–Cu at 1073 K. They also added that Ni–Cu interaction with the support plays an important role in the reaction network. Following this study, Akande et al. [31] modeled the reforming of ethanol to produce hydrogen over 15 wt % Ni/ Al_2O_3 catalyst in a packed bed reactor at atmospheric pressure and within the temperature range of 596 to 793 K. They proposed an Eley Rideal type rate model based on the assumption that dissociative adsorption of ethanol on active sites is the rate determining step.

Some researchers [32], [33] integrated nickel on MgO support and test it for ethanol reforming. Freni et al. [32] produced hydrogen with Ni/MgO catalyst in simulating molten carbonate fuel cell (MCFC) conditions. They concluded that this catalyst exhibits very high selectivity to H_2 and CO_2 . This is because this catalyst has the low tendency to promote carbon monoxide methanation and ethanol decomposition reactions. In addition, coke formation

was strongly depressed because of the benefits induced by the use of the basic carrier which positively modifies the electronic properties of Ni. Following this study, Frusteri et al. [33] investigated the operating conditions of ethanol reforming with Ni/MgO and Ni/CeO₂ catalysts in MCFC. They concluded that addition of oxygen to water-ethanol feed stream is important to decrease coke formation for both systems and high hydrogen selectivity (> 98%) was obtained on both of the catalyst at 650 °C.

Yang et al. [34] studied nickel based catalyst with other type of oxide support ZnO for the steam reforming of ethanol. They compared their catalyst with nickel catalysts supported on La₂O₃, MgO and γ -Al₂O₃ and found out that Ni/ZnO is superior among the catalysts, especially in terms of selectivity and distribution of byproducts. For complete conversion of ethanol they obtained hydrogen selectivity of up to 95% at 650 °C. However, they can not prevent CH₄ formation as side product.

Copper based catalysts also widely used in reforming applications for hydrogen production. Cavallaro and Freni [35] used CuO/ZnO/Al₂O₃ catalyst for ethanol steam reforming. They concluded that high pressure reduces H₂, CO and CO₂ production, while high temperature produces the opposite effect and the catalyst exhibited good activity with CO, CO₂ and H₂ as the main products above 630 K. Nishiguchi et al., [36] studied ethanol reforming with CuO/CeO₂ and they achieved to produce acetone with hydrogen. Amphlett et al., [37] also worked ethanol steam reforming with Cu based catalysts and concluded that CuO/ZnO, CuO/SiO₂, CuO/Cr₂O₃ or CuO/NiO/SiO₂ might be promising for reforming of ethanol–water mixtures at 623–723 K.

The more extended study was performed by Duan and Senkan [38] for steam reforming of ethanol. They evaluated ZrO₂, CeO₂, TiO₂, SiO₂, Al₂O₃ supports by integrating most of the metals in the periodic table, using a combinatorial method. They concluded that Ni, Cu, Pd and Pt are among the most active metals in ethanol steam reforming reaction. In addition, they stated that copper was mainly predominant just in the first stages of the reaction mechanism namely ethanol dehydration and dehydrogenation steps where as

nickel was the phase mainly responsible for the hydrogen production although the copper presence decreased the CO and coke formation.

One of the most recent study done by using Ni and Cu based catalysts was performed by Vizcaino et al. [39]. They used bimetallic Cu-Ni/SBA-15 prepared with different nickel (4–9 wt %) and copper (2–6 wt %) loadings. They pointed that Cu-Ni/SBA-15 sample with 2 and 7 wt % of copper and nickel respectively, exhibited a 77.2% of hydrogen selectivity with a CO_2/CO_x molar ratio of 0.71.

CHAPTER 3

M41S MESOPOROUS MATERIALS

3.1. Mesoporous Materials

Porous materials are classified by IUPAC into three groups depending on their sizes [40]; microporous, mesoporous and macroporous materials. As it is understood from the naming of the groups, the mesoporous materials having pore size between 20-500 Å and between the microporous materials having pore size smaller than 20 Å and the macroporous materials having pore size larger than 500 Å.

Microporous materials such as zeolites were the major materials used within the industrial areas such as oil refining, petrochemistry and synthesis of chemicals because of their high surface area, sharp selectivity for the reactants and control of the adsorption properties. Besides their advantageous properties, they are not able to efficiently process molecules that are larger than their pore diameters (maximum 10-12 Å) [41]. Consequently, it has been a long search for synthesis methods that will increase the pore size of the zeolites, and at the same time retain the crystalline framework of them.

The discovery of M41S family of materials was the solution of this limitation of zeolites and also it initiated the mesoporous materials decade.

3.2. M41S Family

M41S family that is composed of three members; MCM-41, MCM-48 and MCM-50 was first introduced in 1992 by Mobil researchers [42]. MCM denotes to Mobil Composition Matter where as the numbers given next to “MCM” name is the batch number. These mesoporous materials having uniform channels ranging from 1.5 to 10 nm also have high surface area values higher than 800 m²/grams and each of the M41S family members has different structures. These materials are fundamentally different from zeolites by the fact that the pore walls are amorphous. The ordering lies in the pore arrangements.

Surfactant/silica ratio also plays crucial role in the determination of the materials’ structure. The schematic representation of this property is given in Figure 2.

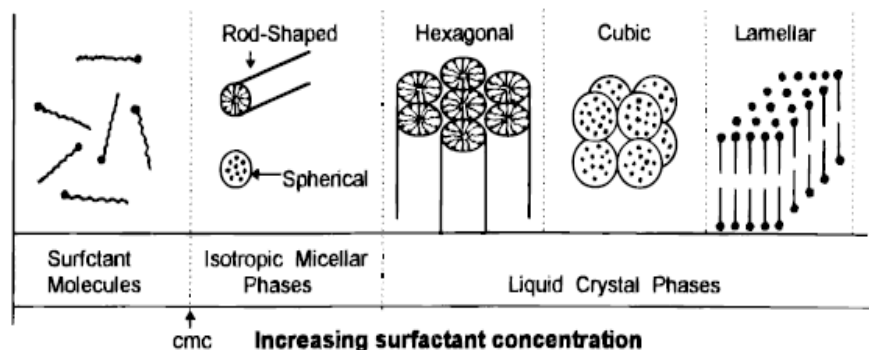


Figure 2. Phase sequence of water- surfactant binary system [43]

As seen in the Fig. 2, when the surfactants are considered in a water-surfactant binary system, at low concentrations they energetically exist as monomolecules. Surfactant molecules aggregate together to form micelles in order to decrease the system entropy as the concentration of surfactant

increases. If concentration continues to increase, hexagonal close packed arrays appear, producing the hexagonal phases [44].

The detailed properties of M41S family members are presented in the following sections.

3.2.i. MCM-41

Among all the M41S members, MCM-41 received much more attention than the others because of its interesting unidirectional, hexagonal honeycomb like structure as shown in the schematic representation in the Fig. 3.a and TEM image in Fig.3.b.

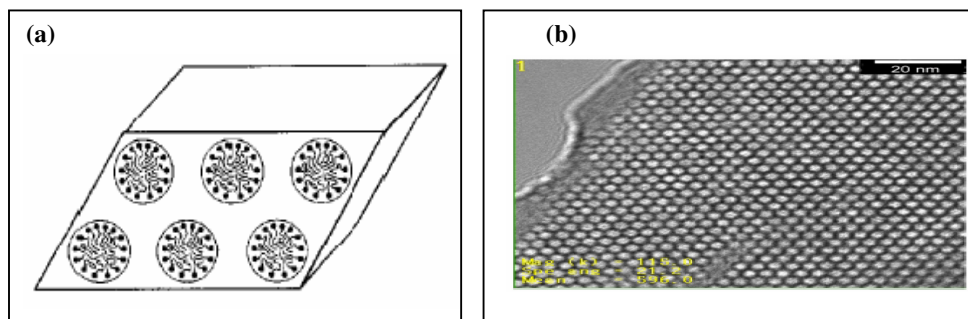


Figure 3.(a) The front view of the MCM-41 uni-directional channels [45], (b) TEM image of the MCM-41 [46]

Main components of MCM-41 are a source of silica, structure-directing surfactants, a solvent and acid or base [41]. Moreover, further studies [47] showed that the relative concentrations of the species present in the synthesis solutions were very important for the final pore structure. It is also added that the pore diameter of MCM-41 increases as the chain length of the surfactant increases.

Although there were many researches introducing modified synthesis methods, Beck et al., [42] proposed the main formation mechanism of MCM-41, namely liquid crystal templating mechanism (LCT) and an alternative mechanism involving the addition of silicate to surfactant molecules giving ordered silicate encased surfactant micelles (Figure 4).

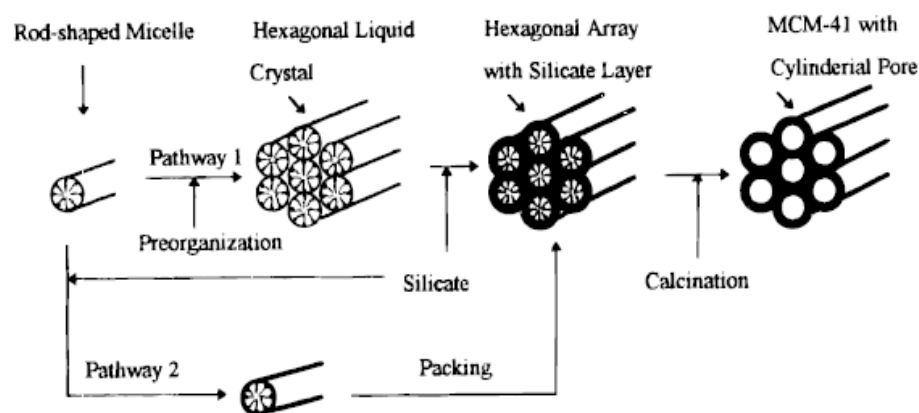


Figure 4. Schematic model of liquid crystal templating mechanism via two possible pathways [42]

As seen from the Fig. 4, the whole process may be via two possible mechanistic pathways:

- (1) The liquid crystal mesophases may form prior to the addition of silicate species
- (2) The silicate species added to the reaction mixture may influence the ordering of the isotropic rod like micelles to the desired liquid crystal phase, i.e., hexagonal mesophase.

When the studies performed about the formation mechanism of MCM-41 is considered, it must be noted that the majority of reports regarding LCT mechanism have been investigated in a system containing relatively large amounts of surfactant (generally more than 10 wt % of the total mixture) [48].

3.2.ii MCM-48

Another M41S family member, MCM-48, is also a good candidate for the catalytic applications because of its cubic structure (Figure 5) indexed in the space group $Ia3d$, of recently modeled as a gyroid minimal surface [49], [50]. Interesting physical properties of MCM-48 are its high specific surface area up to $1600 \text{ cm}^2/\text{g}$, specific pore volume up to $1.2 \text{ cm}^3/\text{g}$ and high thermal stability [51]. The catalytic properties can be adjusted by the incorporation of different metals.

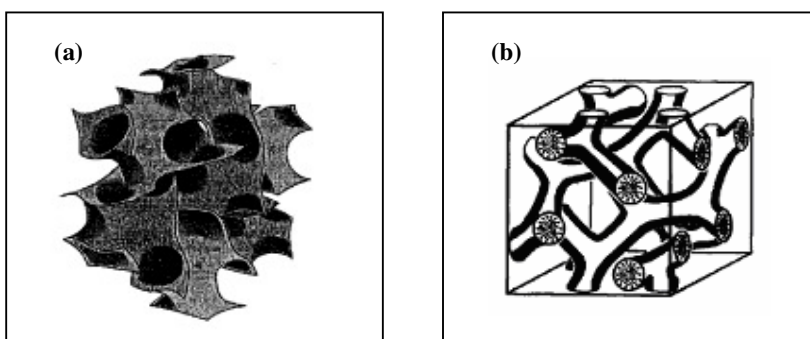


Figure 5. (a) The proposed 3D view of MCM-48 structure [52], (b) The schematic representation of proposed model of MCM-48 [45]

Although MCM-48 has very attractive pore structure, the synthesizing it on a large scale has some drawbacks. Huo et al., [53] produced MCM-48 using alkoxide-based organic silica sources, such as tetraethylorthosilicate ($\text{Si}(\text{OC}_2\text{H}_5)_4$ or "TEOS") or its homologues. These reagents, however, present significant handling problems (e.g., high toxicity, moisture sensitivity) and are costly, making large-scale synthesis of crystalline MCM-48 by this procedure impractical [54].

Due to the difficult, expensive, elusive, and not consistently reproducible synthesis procedures used for the synthesis of MCM-48, the usage of this material was not preferable [54].

3.2.3. *MCM-50*

Unlike the other M41S family members, MCM-50 has a lamellar arrangement of surfactant and silica layers as shown in the below Figure 6. However it is very unstable that the structure of MCM-50 collapses upon calcinations and does not give a mesoporous compound [45].

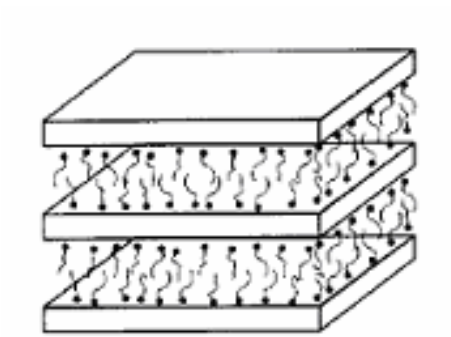


Figure 6. The schematic representation of MCM-50 [45]

3.3. Characterization of Mesoporous material MCM-41

3.3.i. X-Ray Diffraction

XRD is a characterization technique that gives information about the crystal structure of the material. This technique play crucial role especially in analyzing the structure of the ordered materials like MCM-41. The studies done to characterize the two dimensional hexagonal structure of MCM-41 showed that MCM-41 characteristically have a sharp (100) plane diffraction peak and the diffraction peaks of higher Miller Index planes, (110), (200) and (210) [42].

3.3.ii. N₂ Physisorption

This method is significant in order to characterize the porous materials. Yao, [55] stated that for MCM-41 type mesoporous materials, there is a sharp step in the mesopore range of $P/P_0=0.2$ to 0.5 at the resulting isotherm, which represents the liquid condensation of N₂ in the uniform mesopores. Moreover he added that the sharper the step of the isotherm the more uniform the pore size is.

3.3.iii. Scanning Electron Microscopy and Energy Dispersive Spectroscopy

This technique is used to monitor the morphology of the material. SEM may be operated differently such as low voltage, surface sensitive; high beam current and high resolution modes depending on the goal of the investigation. The spatial resolution of the SEM depends on the size of the electron spot which in turn depends on the magnetic electron-optical system which produces the scanning beam. The resolution is also limited by the size of the interaction volume, or the extent to which the material interacts with the electron beam [56].

EDS is a standard procedure for identifying and quantifying elemental composition of sample areas as small as a few cubic micrometers. The characteristic X-rays are produced when a material is bombarded with electrons

in an electron beam instrument, such as a scanning electron microscope (SEM). Detection of these x-rays can be accomplished by an energy dispersive spectrometer, which is a solid state device that discriminates among X-ray energies.

3.4. Studies from Literature about Cu-MCM-41 and Ni-MCM-41 Type Catalytic Materials

There are many studies focused on the metal incorporated MCM-41 catalysts prepared by various techniques. In the scope of this study, the literature about copper and nickel incorporated MCM-41 type catalysts was dealt.

Different researchers applied different synthesis recipes for the preparation of Cu-MCM-41 type catalytic materials and applied these catalysts to different reactions. Velu et al., [57] synthesized Cu-MCM-41 type catalysts having Cu content below 4 wt.% at room temperature by the method of direct insertion of metal ions and used these catalysts for methanol and ethanol partial oxidation. They reported that copper amount of above 3.02 wt % would result in the collapse of the ordered mesoporous framework of MCM-41 and the copper ions are located in a readily accessible position, likely in the interior surface of the mesopores of the Cu-MCM-41. They also stated that the catalytic partial oxidation of methanol and ethanol over the copper containing MCM-41 materials yield selectively formaldehyde and acetaldehyde. On the contrary, by applying novel coassembly route at 273 K, Guo et al.,[58] achieved to synthesize Cu-MCM-41 materials having up to 16.8 copper wt. % percent. Moreover Wan et al., [59] synthesized Cu-Al-MCM-41 by modified hydrothermal method. Noreña-Franco et al., [60] studied the hydroxylation of phenol by using Cu-MCM-41 catalyst and found out that the Cu-MCM-41 synthesized by impregnation method had high selectivity to catechol.

Nickel was also integrated on MCM-41 structure by different methods to be used for different catalytic applications. An example can be given from the study of Wojcieszak and his co-workers [61] that they prepared Ni-MCM-

41 and Ni/Al-MCM-41 samples via wet impregnation method including 1.7–5 wt. % nickel content and tested these catalysts at the gas-phase benzene hydrogenation reaction. More recent studies about Ni-MCM-41 preparation and catalytic applications were performed by Du et al., [62] and Li et al., [63]. Du et al, [62] produced 1-3 wt. % Ni integrated MCM-41 samples which they prepared by using 16 carbon alkyl template. They used these catalysts for the methanation of the carbon dioxide and concluded that significant selectivity to methane (85.1%) was obtained with 1 wt% Ni-MCM-41 at a reaction temperature 573 K. Li et al., [63] used bimetallic Ni-W-MCM-41 catalysts for the hydrodesulfurization and hydrogenation reactions and also present Na⁺ and K⁺ ions in order to see their effect on the catalytic activity. They proposed that the introduction of Na⁺ and K⁺ strongly inhibits the hydrogenation activity, but enhances the hydrogenolysis activity of Ni–W/MCM-41 catalysts. Nalbant et al., [64] prepared Ni and Cu incorporated materials by direct hydrothermal synthesis and the impregnation procedures and concluded that these materials showed highly attractive pore structure and surface area results for catalytic applications.

3.5 Objectives of the Study

Hydrogen, burning clean and having the highest energy content, is the alternative energy carrier to the fossil based fuels. Due to the transportation and storage difficulties of hydrogen hydrocarbon processing fuel cells gained importance. Among the hydrocarbons, alcohols easily decompose to give hydrogen rich mixture. Up to now, many researchers dealt with methanol reforming however the toxicity problem of methanol could not be solved. Unlike methanol, ethanol is low in toxicity. Advantageous properties of ethanol such as being renewable, easy to transport and cheap make it an attractive resource for fuel cell applications.

The Ni-MCM-41 and Cu-MCM-41 catalysts prepared with different techniques showed high activities for various reactions. As described in Chapter 2, nickel and copper containing catalysts showed good performances

for the steam reforming of ethanol. For this reason in this study it was aimed to prepare Ni-MCM-41 and Cu-MCM- 41 catalysts and test these materials for steam reforming of ethanol reactions. The effect of reaction parameters (temperature, space time) and catalyst properties (metal loading, preparation method) were investigated.

CHAPTER 4

EXPERIMENTAL

In this study, two Ni-MCM-41 type catalysts with different nickel loadings and two Cu-MCM-41 type catalysts with different preparation techniques were used in steam reforming reaction of ethanol to produce hydrogen. The catalysts synthesized during this study were prepared by High Temperature Direct Synthesis Method. In addition, one Cu-MCM-41 type catalyst which was prepared by impregnation method by Nalbant [64] was also used in the steam reforming reactions.

4.1. Catalyst Preparation

4.1.i. Chemicals

Through the preparation of metal incorporated MCM-41 type catalysts mainly five components are required:

- Sodium silicate solution (27 wt. % SiO₂, 14 wt. % NaOH) from Aldrich as a source of silica
- Hexadecyltrimethylammonium bromide (CTMABr, 99 % pure powder) from Merck as a source of surfactant
- Deionized water from Millipore Ultra-Pure Water System as a source of solvent

- Sulfuric acid (H_2SO_4) from Merck as a source of acid
- Nickel (II) nitrate hexahydrate ($\text{Ni}(\text{NO}_3)_2 \cdot 6\text{H}_2\text{O}$) from Merck and Copper (II) nitrate trihydrate ($\text{Cu}(\text{NO}_3)_2 \cdot 3\text{H}_2\text{O}$) from Merck as sources of metals.

4.1.ii. Preparation of Ni-MCM-41 by High Temperature Direct Synthesis Method

Ni-MCM-41 catalyst was prepared by using a direct hydrothermal synthesis method, which was also employed in our recent studies in the preparation of Pd-MCM-41 and V-MCM-41 catalysts [65]-[66]. The synthesis was initiated by desolving 13.2 g of hexadecyltrimethylammonium bromide (CTMABr) surfactant in 87 ml deionized water by continuous mixing at 30°C for 1 hour. This was followed by the addition of 11.3 ml sodium silicate dropwise into the solution with continuous stirring. Then certain amount of nickel (II)-nitrate hexahydrate ($\text{Ni}(\text{NO}_3)_2 \cdot 6\text{H}_2\text{O}$) (0.67 g for Ni/Si mole ratio of 0.032 and 2.05 g for Ni/Si mole ratio of 0.10) was added to the solution. The final pH of this solution was adjusted to 11 by sulfuric acid. After these steps, a gel mixture was obtained and mixed for 1 hour. At the end of mixing, the mixture was taken into a teflon-lined stainless steel autoclave in which the hydrothermal synthesis took place for 96 h at 120 °C. The solid product was then filtered and washed several times until the pH of the wash liquid was set to a constant value (pH:7.0). The resulting product was dried at 40°C and calcined in a tubular furnace in a flow of dry air. The furnace was heated to 550°C at a heating rate of 1°C/min and then calcination was continued at this temperature for 6 h.

Two Ni-MCM-41 type catalysts were prepared and labeled as Ni-HT (I) and Ni-HT (II). The difference of these catalysts was their nickel loadings that Ni-HT (I) was composed of Ni/Si (mole) = 0.032 whereas, Ni-HT (II) was composed of Ni/Si (mole) = 0.10 in the solution.

The schematic representation of the procedure is given in Figure 7.a

4.1.iii. Preparation of Cu-MCM-41 by High Temperature Direct Synthesis Method

The procedure of Cu-MCM-41 synthesis by this method is similar to the synthesis procedure of Ni-MCM-41 by high temperature direct synthesis method described in the previous section. The first task was to prepare solution of 87 ml deionized water with 13.2 g hexadecyltrimethyl ammonium bromide. The solution was heated to 30°C and waited for complete dissolution. Afterwards, 11.3 ml sodium silicate was dropped into the solution. Copper (II) nitrate trihydrate (1.7 g solid in 1 ml water) solution was added to the resulting gel mixture to produce catalyst with a Cu/Si (mole) ratio of 0.1 with continuous stirring. This is followed by the addition of sulfuric acid to adjust the pH of the sample to 11. The mixture was then taken into teflon-lined stainless steel autoclave in which the hydrothermal synthesis took place for 96 h at 120 °C. The solid product was then filtered and washed several times until the pH of the wash liquid was set to a constant value (pH:7.0). The resulting product was dried at 40°C and calcined in a tubular furnace in a flow of dry air. The furnace was heated to 550°C at a heating rate of 1°C/min and then calcination was continued at this temperature for 6 h. The resulting product is named as Cu-HT (I).

The schematic representation of the procedure is given in Figure 7.a

4.1.iv. Preparation of Cu-MCM-41 by Impregnation Method

The Cu-MCM-41 synthesized by the impregnation method by Nalbant [64] was started by the preparation of MCM-41 type catalytic material. 13.2 g hexadecyltrimethyl ammonium bromide was mixed with 87 ml of deionized water, heated up to 30°C and stirred until complete dissolution has occurred. Then, 11.3 ml sodium silicate was added to the solution with continuous mixing. After addition of sodium silicate the ph of mixture was set to 11 with sulfuric acid. The 1 hour stirred mixture was then taken to teflon-lined stainless

steel autoclave in which the hydrothermal synthesis took place for 96 h at 120 °C. The solid product was then filtered and washed several times until the pH of the wash liquid was set to a constant value. The resulting product was dried at 40°C. Uncalcined MCM-41 material was then mixed with 0.67 g of copper (II) nitrate trihydrate in 11 ml deionized water. The liquid phase of the mixture was removed by centrifugation and the obtained product was dried at room temperature and then under vacuum for one night. The resulting product was finally calcined at 550°C for 6 hours in a flow of dry air. The resulting sample was identified as Cu-Imp (II).

The schematic representation of the method is also given in Figure 7.b.

4.2. Catalyst Characterization

The materials prepared with the procedures explained in the previous sections were analyzed by X-ray diffraction (XRD), energy dispersive spectroscopy (EDS), nitrogen physisorption, scanning electron microscopy (SEM) and temperature programmed reduction (TPR) techniques.

4.2.i. X-Ray Diffraction (XRD)

The XRD patterns of the synthesized materials were obtained by Rigaku D/MAX2200 diffractometer in Metallurgical and Materials Engineering at METU.

4.2.ii. Energy Dispersive Spectroscopy (EDS)

Bulk compositions of the materials were determined by JEOL 6400 apparatus at METU. For the analysis of the samples, materials were coated with gold.

4.2.iii. Nitrogen Physisorption

Surface area (BET), isotherms and pore size distribution data were obtained by Quantachrome Corporation, Autosorb-1-C/MS at METU Central Laboratory. The samples were dried at 110 °C for one night before the analyses. The characterization results also led to the calculation of the pore diameters and pore wall thicknesses.

4.2.iv. Scanning Electron Microscopy (SEM)

The SEM images showing the morphologies of the materials were taken by JEOL 6400 apparatus at METU Material Science and Metallurgical Engineering Department.

4.2.v Temperature Programmed Reduction (TPR)

TPR analysis of Ni-HT (I) was performed by using a Hiden analytical quadrupole mass spectrometer attached to a temperature controlled tubular reactor including 73 cm long, 17 mm diameter quartz tube which was used as tubular reactor. The end of the tubular reactor was connected to helium and hydrogen gas. The gas stream flowing through the reactor filled with the 0.2 g powder sample had a composition of 5% H₂ in He whereas the inlet total flow of the gas was 50 ml/min. The reduction of the sample was achieved by heating the material up to 575°C with a heating rate of 5°C/min.

4.3. Steam Reforming Reaction Set-up

Before testing synthesized materials for the reaction, the synthesized catalyst Ni-HT (I) and Ni-HT (II) were reduced with hydrogen gas at 550°C (10°C/min) for 5 hours whereas the Cu-HT(I) and Cu-Imp (II) samples were reduced at 450°C (10°C/min) for 3 hours. The reduced catalyst was placed in a

quartz reactor which was placed into a tubular furnace and isolated in order to avoid the heat losses. The reaction temperature was controlled by the temperature controller of the furnace. Liquid feed was adjusted to a $\text{H}_2\text{O}/\text{C}_2\text{H}_5\text{OH}$ molar ratio of 3.2 (50 liq. vol. %). The prepared feed solution was injected to the system by Waters 510 HPLC injection pump, at 0.1 ml/min for the Ni-HT(I) sample and by Cole Parmer liquid injection pump, at 1.8 ml/hr for the rest of the catalysts (Ni-HT(II), Cu-HT(I), Cu-Imp (II)). This liquid stream was evaporated in the evaporator (at 150°C) in which ethanol-water vapor was mixed with an inert gas (Ar for Ni-HT (I) or He for Ni-HT (II), Cu-Imp (II) and Cu-HT (I)) to adjust the composition to a desired value. The total flow rate of the gas stream was 140.18 mL/min (measured at 423 K). The gas analysis at the reactor outlet was carried out by a gas chromatograph (Agilent Technologies 6850) which was connected on-line to the reactor outlet stream. During the analysis of Ni-HT (I) catalyst, the chromatograph was equipped with a CTR column (Altech) and during the Ni-HT (II), Cu-HT (I), Cu-Imp (II) catalysts' analyses Porapak S column (Altech) was used in the chromatograph. The CTR column contains two columns placed one inside of the other where the outer column is 6 ft packed with activated molecular sieve; the inner column is 6 ft porous polymer mixture. The detector used was thermal conductivity detector (TCD) and the two different oven temperature programme was applied to analyze the gases. The programme information of GC is given in Table 1 and the parameters set in the GC are given in Table 2. Argon was used as both the carrier gas and the reference gas for the Ni- HT (I) analysis whereas helium was employed as carrier gas and reference gas for the Ni-HT(II), Cu-HT(I), Cu-Imp (II) catalysts analyses. Flow rate of the carrier gas was controlled by a mass flow controller. The real image and the schematic representation of the reaction set-up is given in Fig.8 and Fig.9.

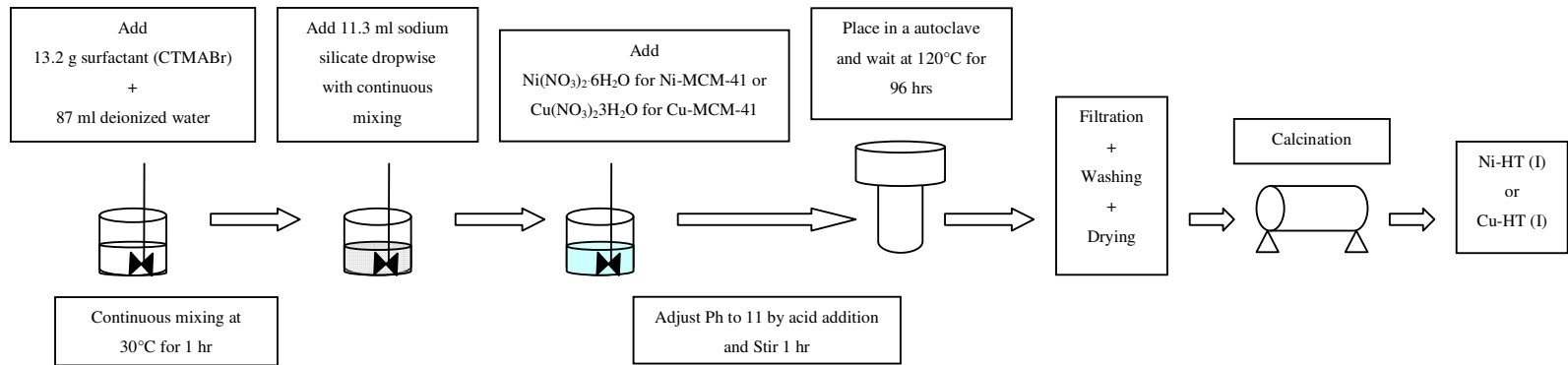
Table 1. The programme information of the Gas Chromatograph

Programme number	Programme Details	Applied catalysts
1	At 30°C For 8 min. $\xrightarrow{\text{ramp}=150^\circ\text{C}/\text{min}}$ At 100°C For 14 min. $\xrightarrow{\text{ramp } 10^\circ\text{C}/\text{min}}$ At 140°C For 9 min.	Ni-HT (I)
2	At 30°C For 3 min. $\xrightarrow{\text{ramp}=20^\circ\text{C}/\text{min}}$ At 175°C For 2 min.	Ni-HT (II) Cu-HT (I) Cu-Imp(II)

Table 2. The set points of the parameters of GC

Parameter	Set Point
Front inlet temperature	200°C
Front inlet pressure	22.5 psi
Reference flow	40 ml/min
Front detector temperature	200°C

(a) High Temperature Direct Synthesis Method



(b) Impregnation Method

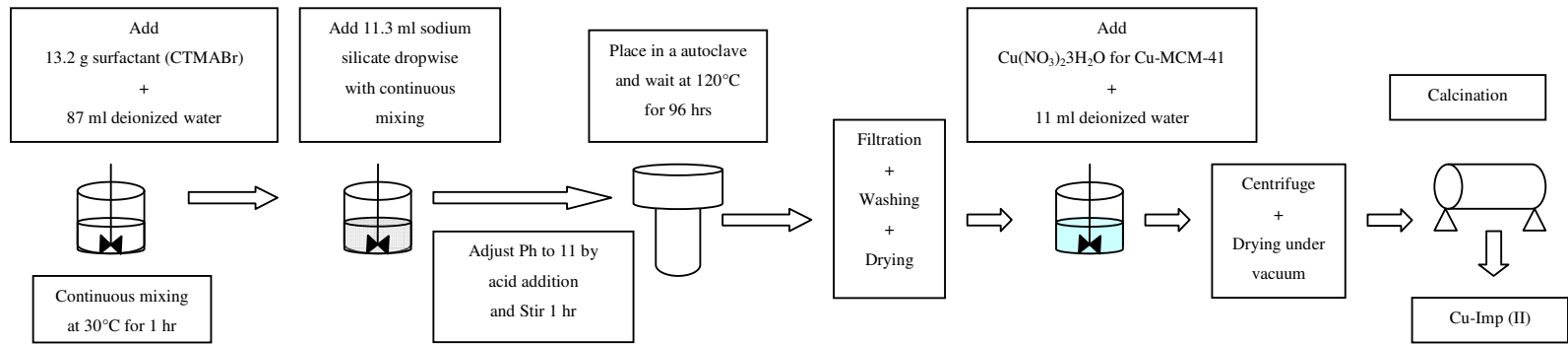


Figure 7. Schematic representation of (a) high temperature direct synthesis method, (b) impregnation method



Figure 8. The real image of reaction set-up

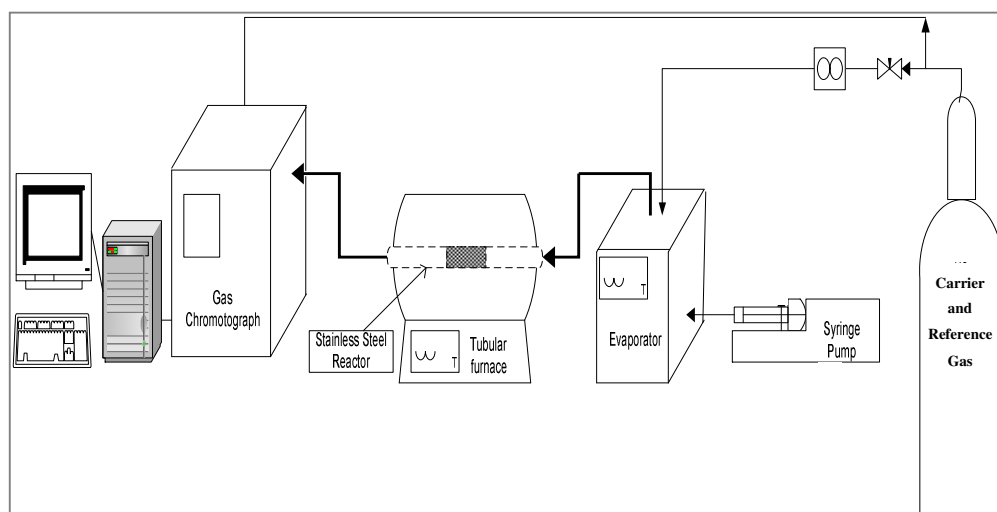


Figure 9. Schematic representation of the reaction set-up

CHAPTER 5

RESULTS AND DISCUSSIONS

In this study, two Ni-MCM-41 samples (Ni-HT (I) and Ni-HT (II)) synthesized by high temperature direct synthesis method having different metal loadings and two Cu-MCM-41 samples (Cu-HT (I) and Cu- Imp (II)) having same metal loading but prepared by different methods namely, high temperature direct synthesis method and impregnation method were characterized by different characterization techniques and tested in the steam reforming reaction of ethanol. The results of these works are given and evaluated under two main sections; Characterization of the Catalysts and Steam Reforming of Ethanol via Ni-MCM-41 and Cu-MCM-41 Catalysts.

5.1. Characterization of Catalysts

The synthesized materials were analyzed by XRD, EDS, SEM, N₂ physisorption and TPR characterization techniques.

5.1.i. XRD

XRD analysis is used to identify the crystal structure of the material and the output of this technique is a diffraction spectrum consisting of a plot of reflected intensities versus the detector angle 2θ . XRD basics were formulized by Bragg's law (Eqn. (1).) as in the following;

$$n\lambda = 2d \sin\theta \quad (1)$$

Bragg's Law was derived by the English physicists Sir W.H. Bragg and his son Sir W.L. Bragg in 1913 to explain why the cleavage faces of crystals appear to reflect X-ray beams at certain angles of incidence (theta, θ). The variable d (d_{100}) is the distance between atomic layers in a crystal, and the variable lambda is the wavelength of the incident X-ray beam and n is an integer [67]. The schematic representation of Bragg's Law is given in the Fig.10.

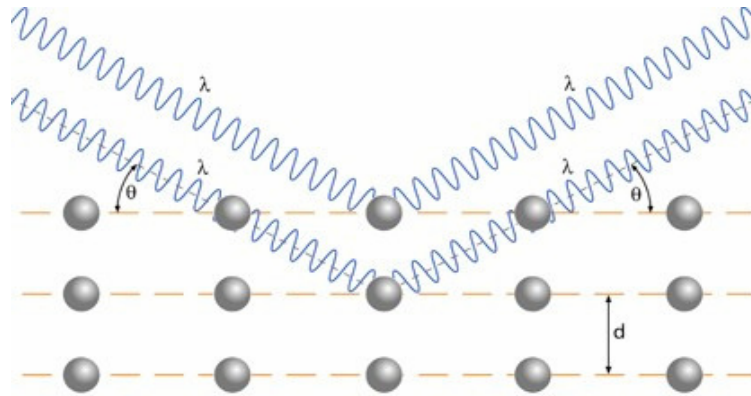


Figure 10. The schematic representation of Bragg's Law [68]

From d_{100} value obtained from the Bragg's Law, one can calculate the lattice parameter "a" by the following Equation (2) [69].

$$a = \frac{2d_{100}}{\sqrt{3}} \quad (2)$$

For the mesoporous materials, the reflection peaks appear at the low-angle range that 2θ value is less than 10 on the diffraction spectrum and these

peaks correspond to the mesopores. According to this information, in this study the XRD analysis were performed for each synthesized catalyst between 2θ angle values of 1-10 degrees and the results of those are given in the Fig. 11-14.

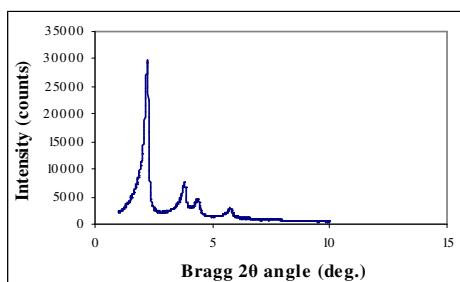


Figure 11. XRD pattern of Ni-HT (I) catalyst

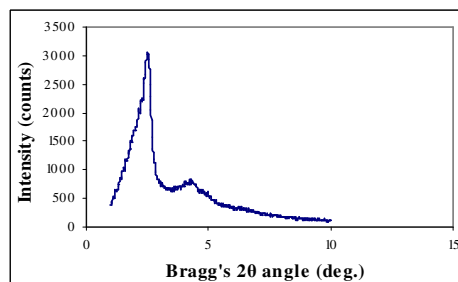


Figure 12. XRD pattern of Ni-HT (II) catalyst

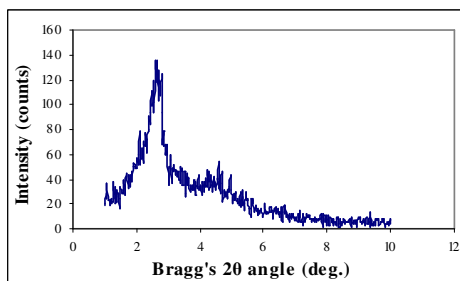


Figure 13. XRD pattern of Cu-HT (I) catalyst

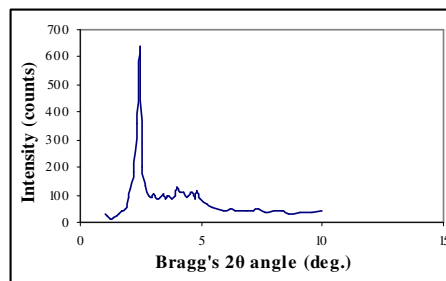


Figure 14. XRD pattern of Cu-Imp (II) catalyst [64]

The XRD pattern of the Ni-HT (I) and Ni-HT (II) synthesized by the one pot hydrothermal procedure that is given in the Fig. 11 and Fig. 12 indicated that the characteristic MCM-41 structure was successfully formed for each sample. The major peaks in the XRD patterns of amorphous MCM-41 formed due to the hexagonal mesostructure of MCM-41. The main XRD peak of Ni-HT (I) corresponding to d_{100} was observed at a 2θ value of 2.23. Also, three of the reflection peaks were observed at 2θ values of 3.82, 4.40 and 5.81. Moreover the main peak of Ni-HT (II) was observed at a 2θ value of 2.56

whereas the reflection peaks were observed at 2θ values of 4.40 and 6.52. It is obvious from the XRD patterns of the two nickel based MCM-41 catalysts that the peaks of Ni-HT (I) sample are more in number, sharper and narrower than the peaks of the Ni-HT (II) sample. As discussed in Section 4.1.ii, Ni/Si atomic ratio within Ni-HT (II) is about five times higher than Ni-HT (I). This can be explained by the fact that as the nickel loading increases the MCM-41 structure is deteriorated.

When the XRD pattern of Cu-HT (I) and Cu- Imp (II) was considered, it can be said that only the main peaks at 2θ value of 2.66 for Cu-HT (I) and 2.45 for Cu-Imp (II) are sharp enough to observe (Fig. 13 and 14). These main peaks indicated that MCM-41 structure was formed. The reflection peaks for Cu-HT (I) are at 2θ values of 4.62 and 6.68 where as for the Cu-Imp (II) the reflection peaks are located at 4.61 and 6.41. When the peaks of the two XRD patterns are compared, it can be said that the peaks of Cu-Imp (II) are narrower and sharper than the peaks of Cu-HT (I).

The calculated ' d_{100} ' and ' a ' values for all catalysts are listed in the below Table 3.

Table 3. d_{100} and a values for the catalysts

Sample ID	d_{100} (nm)	a (nm)
Ni-HT(I)	3.96	4.57
Ni-HT(II)	3.45	3.98
Cu-HT(I)	3.32	3.83
Cu-Imp(II) [64]	3.6	4.2

As seen from the table 3., Ni-HT (I) has the highest 'd₁₀₀' and 'a' magnitude when compared with the values of other prepared samples.

Ni-HT (I) and Ni-HT (II) samples were also analyzed at wider angle range and the results were plotted as in the Fig. 15 and 16.

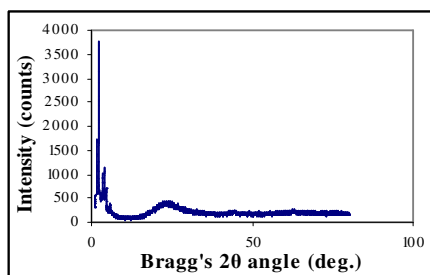


Figure 15. XRD pattern of Ni-HT (I) catalyst wide angle range

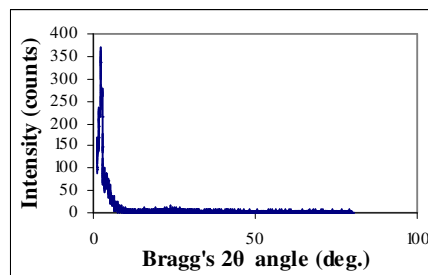


Figure 16. XRD pattern of Ni-HT (II) catalyst (wide angle range)

Ni is considered to be well dispersed into the MCM-41 structure. Absence of sharp XRD peaks at about 2θ values of 37.26 and 43.28 in the wide angle XRD pattern of the synthesized catalyst (Figure 15 and 16) also indicated the absence of large crystalline Ni clusters.

5.1.ii. EDS and SEM

EDS is a standard procedure for identifying and quantifying elemental composition of sample areas as small as a few cubic micrometers as stated in the Chapter 3.3.iii. The results of EDS analyses of Ni-HT (I), Ni-HT (II), Cu-HT (I), Cu-Imp (II) are tabulated in Table 4. The detailed output of the EDS analyses are given in Appendix A.1.

Table 4. EDS analysis of the Ni-HT (I), Ni-HT (II), Cu-HT (I) and Cu-Imp (II)

Sample ID	Element	Weight Conc. % (*)	Atomic Conc. %	M/Si (M= Ni, Cu)		M/Si (M=Ni, Cu) In the solution (Atomic)
				Weight	Atomic	
Ni-HT (I)	Ni	7.00	3.47	0.075	0.036	0.033
	Si	93.00	96.53			
Ni-HT (II)	Ni	23.41	12.75	0.31	0.15	0.1
	Si	76.59	87.25			
Cu-HT (I)	Cu	20.14	10.03	0.25	0.11	0.1
	Si	79.86	89.97			
Cu-Imp (II) [64]	Cu	30.23	16.07	0.43	0.19	0.1
	Si	69.77	83.93			

(*) Oxygen Free Basis

The EDS analysis of the Ni-HT (I) which had a Ni/Si atomic ratio of 0.033 in the solution indicated a Ni/Si atomic ratio of 0.036 in the bulk of the catalyst. From the EDS result of the Ni-HT (II) which had a Ni/Si atomic ratio of 0.1 in the solution during preparation, Ni/Si atomic ratio of 0.15 in the bulk of the catalyst was obtained. Similarly for the copper based catalysts, having 0.1 Ni/Si atomic ratios in the solutions, the EDS analyses gave different Cu/Si ratios in the bulk of the catalysts. The results of the analyses showed that Cu-HT (I) has Cu/Si atomic ratio of 0.11 in the bulk and the Cu-Imp (II) has Cu/Si atomic ratio of 0.19 in the bulk of the catalyst.

These results indicated that Ni and Cu were successfully incorporated into the MCM-41 structure by both direct synthesis and impregnation methods. In fact, higher Ni/Si and Cu/Si ratios in the solid matrix than the corresponding values in the solution indicated loss of some of the Si during the hydrothermal synthesis procedure for the direct synthesis materials.

The SEM analysis of the Ni-HT (I), Ni-HT (II) and Cu-HT (I) were performed in the METU Metallurgical Engineering Department. The SEM images of the Cu-Imp (II) which were taken in TUBITAK were adapted from the Nalbant [64]. Some of the SEM images of the catalysts are given in the Fig.17-20. In Appendix A.2, some other SEM images of these catalysts are also given.

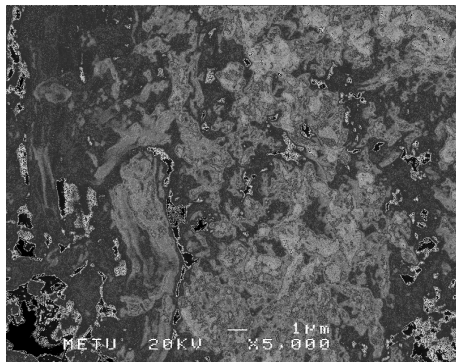


Figure 17. SEM image of Ni-HT (I)

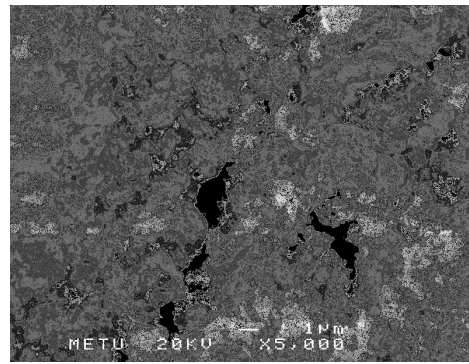


Figure 18. SEM image of Ni-HT (II)

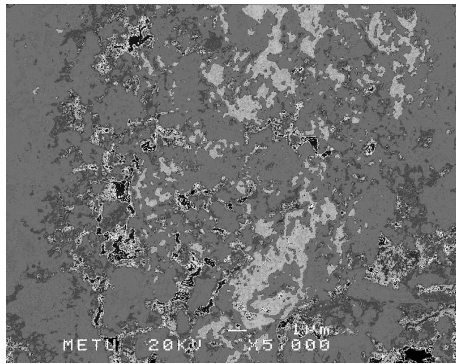


Figure 19. SEM image of Cu-HT (I)

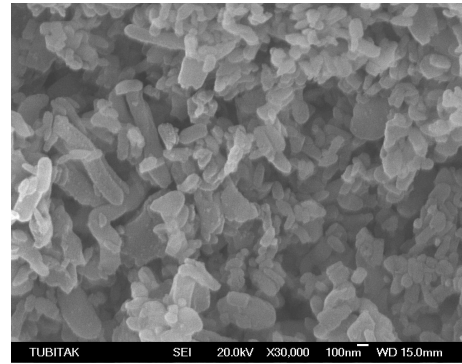


Figure 20. SEM image of Cu-Imp (II) [64]

5.1.iii. N_2 Physisorption

Nitrogen adsorption and desorption isotherms of Ni-HT (I), Ni-HT (II), Cu-HT (I) and Cu-Imp (II) are given in Figures 21-24 in the below.

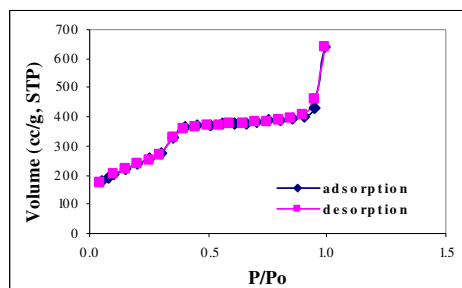


Figure 21. Isotherm of Ni-HT (I)

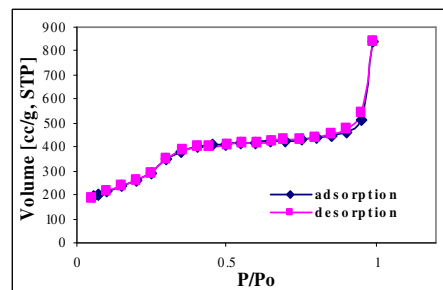


Figure 22. Isotherm of Ni-HT (II)

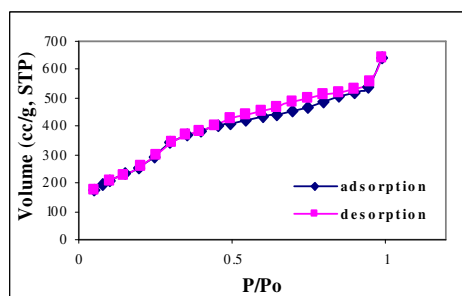


Figure 23. Isotherm of Cu-HT (I)

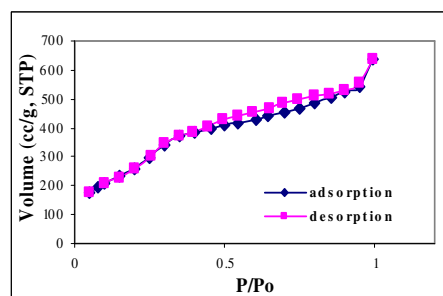


Figure 24. Isotherm of Cu-Imp (II)[64]

Figure 21 and Figure 22 showed that the Ni-HT (I) and Ni-HT (II) materials have typical Type IV isotherms, indicating mesoporous structure. When the Fig. 23 and Fig. 24 are considered, the similar remarks could be addressed. However, for the Cu-HT (I) and Cu-Imp (II) catalysts, the typical

shape of type IV isotherm is not as definite as it is for the Ni-HT (I) and Ni-HT (II).

The pore size distributions of synthesized materials Ni-HT (I), Ni-HT (II), Cu-HT (I) and Cu-Imp (II) are given in the Figures 25-28. These plots are based on the adsorption branch data points.

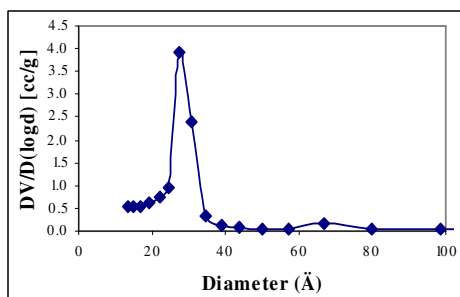


Figure 25. Pore size distribution of Ni-HT (I)

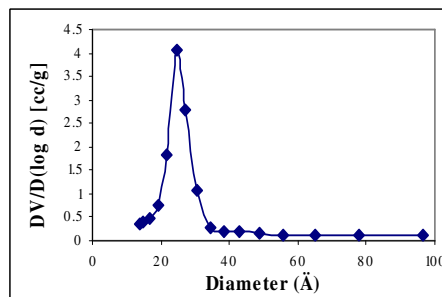


Figure 26. Pore size distribution of Ni-HT(II)

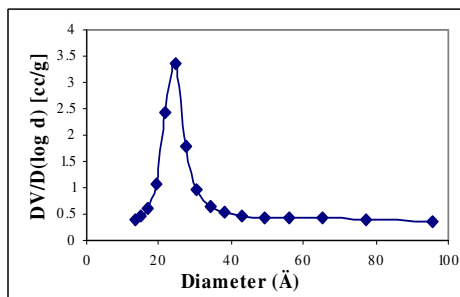


Figure 27. Pore size distribution of Cu-HT (I)

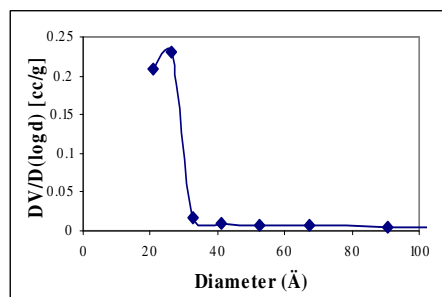


Figure 28 Pore size distribution of Cu Imp (II) [64]

As shown in Figure 25-28 pore size distribution of Ni-HT (I), Ni-HT (II), Cu-HT (I) and Cu-Imp (II) are all quite narrow having pores between 2.2-2.7 nm. According to these figures, the average pore diameter of Ni-HT (I) and Ni-HT (II) were calculated as 2.7 and 2.6 respectively. On the other hand, Fig. 27 and 28 evaluation showed that Cu-Imp (II) has 2.7 nm pore diameter

whereas Cu- HT (I) has 2.5 nm pore diameter. From the pore diameter data one could calculate pore wall thicknesses of the materials by using Equation (3).

$$\delta = a-d_p \quad (3)$$

The pore diameter, pore wall thickness and the BET surface area values of Ni-HT (I), Ni-HT (II), Cu-HT (I) and Cu-Imp (II) are tabulated in Table 5.

Table 5. Pore Diameter, Pore Wall Thickness and BET Surface Area Data of the Synthesized Catalysts

Sample ID	Pore Diameter (nm)	Pore Wall Thickness (nm)	BET Surface Area (m²/g)
Ni-HT (I)	2.7	1.87	861
Ni-HT (II)	2.6	1.38	945
Cu-HT (I)	2.5	1.33	950
Cu-Imp (II) [64]	2.7	1.5	631

As seen from Table 5., BET surface area values of all the materials are higher than 600 m²/g and Cu-HT (I) has the highest BET surface area value of 950 m²/g. For all the direct synthesis materials, surface area values are over 860 m²/g. For the copper based MCM-41 materials, one could say that the material synthesized via impregnation method has lower surface area value than the catalyst synthesized by high temperature direct synthesis method has. This indicated plugging of some of the smaller pores by copper during the impregnation procedure.

For the Ni-HT (II) and Cu-HT (I) that have same metal loading and prepared by the same method, from the Table 5, it is seen that Ni-HT (II) has smaller pore diameter but thicker pore wall than Cu-HT (I) has.

5.1.iv. TPR

TPR analysis was performed only for Ni-HT (I) catalyst and the temperature programmed profile in the Fig.29 was obtained.

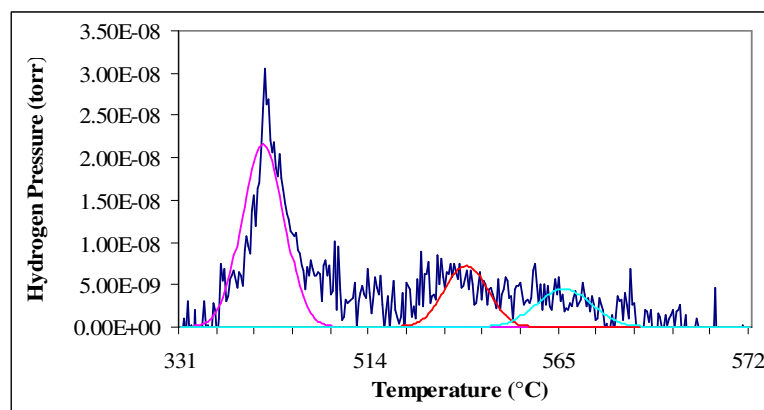


Figure 29. Temperature Programmed Reduction Profile of Ni-HT (I)

Hydrogen temperature programmed reduction of the Ni-HT (I) indicated that most of the nickel in the catalyst was reduced in a temperature range between 360 – 514 °C (Fig.29). Presence of smaller secondary peaks at higher temperatures is considered to correspond to the reduction of nickel present deep in the lattice of MCM-41 structure. The three reduction curves were also shown in Fig. 29.

The summary of the characterization results of the catalysts are given in Table 6.

Table 6. The Summary of the Characterization Results

Sample ID	d₁₀₀ (nm)	a (nm)	M/Si (M= Ni, Cu) weight (EDS)	M/Si (M= Ni, Cu) atomic (EDS)	M/Si (M= Ni, Cu) solution	Pore Diameter (nm)	Pore Wall Thickness (nm)	BET Surface Area (m²/g)
Ni-HT(I)	3.96	4.57	0.075	0.036	0.033	2.7	1.87	860.5
Ni-HT(II)	3.45	3.98	0.31	0.15	0.1	2.6	1.38	944.9
Cu-HT(I)	3.32	3.83	0.25	0.11	0.1	2.5	1.33	950.1
Cu-Imp(II) [64]	3.6	4.2	0.43	0.19	0.1	2.7	1.5	631

5.2. Steam Reforming of Ethanol via Ni-MCM-41 and Cu-MCM-41 Catalysts

The synthesized materials Ni-HT (I), Ni-HT (II), Cu-HT (I) and Cu-Imp (II) were tested for steam reforming reaction of ethanol. The reaction parameters for each of the catalyst are tabulated in Table 7.

Table 7. The summary of reaction parameters of Ni-HT (I), Ni-HT (II), Cu-HT (I) and Cu-Imp (II)

Sample ID		Carrier & Reference Gas in GC	Temperature (°C)	$\frac{\text{H}_2\text{O}}{\text{EtOH}}$ (mole)	EtOH + H ₂ O Flow (ml/min)	Total Flow (ml/min) (at STP)	Amount packed to the Reactor (g)	Space time (s.g/ml)
Ni-HT (I)	a	Ar	300-550	3.2	126.1	140	0.0567	0.024
	b						0.15	0.068
Ni-HT (II)		He	300-550	3.2	40	140	0.15	0.068
Cu-HT (I)		He	300-550	3.2	40	140	0.15	0.068
Cu-Imp (II)		He	300-550	3.2	40	140	0.15	0.068

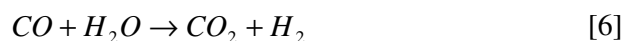
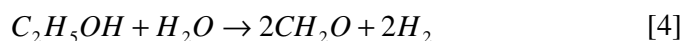
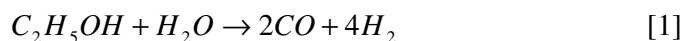
From Table 7, it is evident that during the reaction experiments the space time and loading effects were observed for the nickel based MCM-41 catalysts and the influence of preparation technique was determined for the copper based MCM-41 catalysts. Moreover the impact of metal type was also understood from the reaction results of Ni-HT (II) and Cu-HT (I). These

significant outcomes are given and discussed in more detail in the following sections; Catalytic activity of nickel based MCM-41 type catalysts, catalytic activity of copper based MCM-41 type catalysts and the comparison of nickel based MCM-41 and copper based MCM-41 catalysts for steam reforming of ethanol.

5.2.i. Catalytic Activity of Nickel Based MCM-41 type catalysts

The reactions performed at atmospheric pressure and the conditions given in Table 7 for Ni-HT (I) and Ni-HT (II) gave main products of hydrogen (H₂) and carbonmonoxide (CO). Depending on the reaction temperature, formaldehyde (CH₂O, at lower temperatures) and methane (CH₄, at higher temperatures) were also observed. Trace amounts of carbondioxide (CO₂) and ethylene (C₂H₄) also formed during reactions.

A possible reaction sequence depending on the products mentioned was proposed and given in the below as Rxn. [1], Rxn. [2], Rxn [3], Rxn [4], Rxn [5], Rxn [6] and Rxn [7]. In the following sections, the reasons of proposing this set of reactions will be discussed in more detail.



As given in Table 7, the Ni-HT (I) was used for steam reforming at two different space times (0.024 s.g/ml and 0.068 s.g/ml) and Ni-HT (II) was used at only one space time (0.068 s.g/ml). The evaluation and discussion of the reaction results of these catalysts will be given together and in order to avoid

confusion, Ni-HT (I) loaded 0.0567 g to the reactor having space time 0.024 s.g/ml was named as Ni-HT (I)a where as Ni-HT (I) loaded 0.15 g to the reactor having space time 0.068 s.g/ml was labeled as Ni-HT (I)b (Table 7).

Mainly, the results of Ni-HT (I)a and Ni (I)b will be compared to understand the effect of space time to the reaction and Ni-HT (II) will be checked against Ni-HT (I)b in order to find out the effect of the Ni/Si ratio on the reaction.

5.2.i.a. Conversion of Ethanol

The conversion of ethanol was defined as follows;

$$X_{EtOH} = \frac{\text{Moles of EtOH converted}}{\text{Moles of EtOH fed to the reactor}} \quad (4)$$

The change of conversion of ethanol with respect to the reaction temperature for Ni- HT (I)a, Ni-HT (I)b and Ni-HT (II) was plotted in Figure 30.

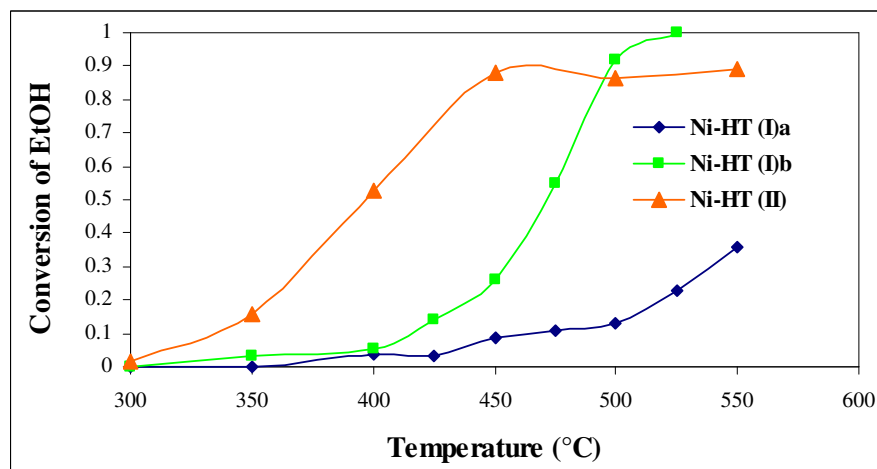


Figure 30. Variation of conversion of ethanol with temperature

As shown in Figure 30, ethanol conversion increased with an increase in temperature, reaching to 0.36 for Ni-HT (I)a and almost complete conversion for Ni-HT (I)b over 500°C. This situation of the two catalysts Ni-HT (I)a and Ni-HT (I)b, having only space time differences, showed that the increase in the space time enhanced the conversion of the reactant ethanol. On the other hand, the conversion of ethanol had a value of 0.9 at 550°C for Ni-HT (II) catalyst. When the conversion trend of Ni-HT (II) compared with the conversion trend of Ni-HT (I)b, it can be said that although the maximum conversion value of Ni-HT (II) is lower, the conversion values of it is much higher in the temperature range of 300-500°C. For instance, at 350 °C, 16 percent of ethanol converted by Ni-HT (II) while there was no reaction happening by Ni-HT (I)b. So the increase of the Ni/Si ratio resulted an increase in the activity of the Ni-MCM-41 type catalyst in the temperature of 300-500°C. To have an activity at temperatures as low as 350°C, is an advantage of the Ni-HT (II) catalyst. A conversion value of about 0.9 was also achieved at about 450°C with this catalyst. Not further increase of conversion at higher temperatures may be due to the formation of some coke on this highly active catalyst, which would decrease its activity.

5.2.i.b. Yield of hydrogen

The definition of hydrogen yield is given in the Eqn. (5).

$$Y_{H_2} = \frac{\text{Moles of hydrogen produced}}{\text{Moles of EtOH fed to the reactor}} \quad (5)$$

The variation of hydrogen yield with temperature is given in the Figure 31.

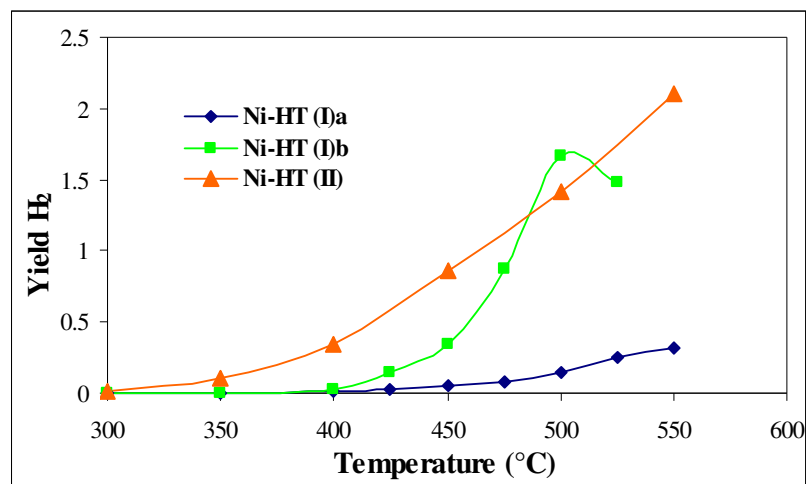


Figure 31. Variation of hydrogen yield with temperature

It can be seen from Fig. 31 that, hydrogen yield values showed an increase with temperature for three cases. At 500°C, a hydrogen yield value of about 1.7 was obtained by using Ni-HT (I)b whereas this value was only 0.3 for Ni-HT (I)a. The hydrogen yield values of the reactions performed with Ni-HT (I)a are lower than the hydrogen yield values obtained from the reactions done with Ni-HT (I)b. By this means, the increase in space time increased the hydrogen yield. For the Ni-HT (II) case, the hydrogen yield reached to a maximum of 2.1. When the hydrogen yields obtained by using Ni-HT (II) and Ni-HT (I)b were compared, during the reaction catalyzed by Ni-HT (II) higher hydrogen yields were obtained which means that the increase in Ni/Si ratio resulted an increase in the hydrogen yield. However, still the hydrogen yield values are lower than the values predicted by Rxn [1]. This is simply due to the formation of some side products like methane and formaldehyde. Further increase in space time may be needed for further increase in hydrogen yield.

5.2.i.c. Selectivity of Side Products

The selectivity of a product was defined in Equation (6).

$$\text{(Selectivity of product A)} S_A = \frac{\text{Moles of A formed}}{\text{Moles of EtOH converted}} \quad (6)$$

With the definition given in the Eqn.(6), selectivity of CO, CH₂O, CH₄, CO₂ and C₂H₄ were calculated. The change of the selectivity of CO with respect to temperature is given in Fig.32.

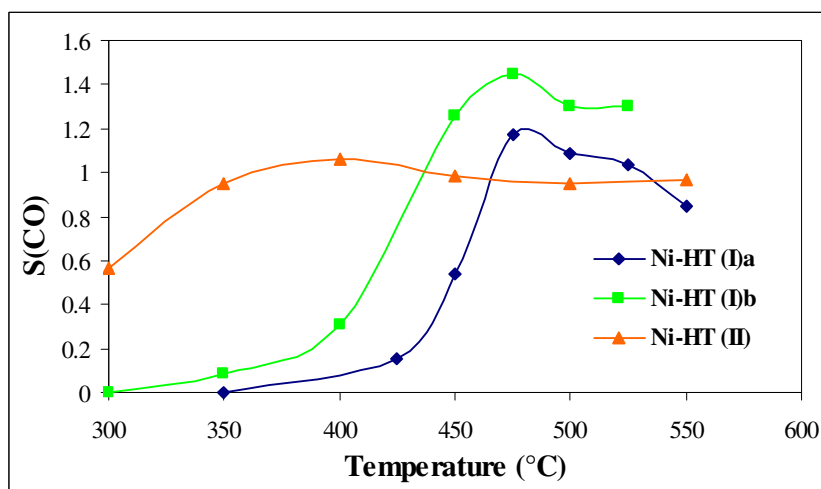


Figure 32. The variation of selectivity of CO with temperature

The selectivity of CO showed an increasing trend with an increase of temperature (Figure 32) for three catalysts, however the increasing trend of Ni-HT (II) was not appeared to be as sharp as they were for Ni-HT (I)a and Ni-HT (I)b. The selectivity of CO reached to about 1.5 over 450°C for Ni-HT (I)b while the selectivity of CO reached to 1.2 at same temperature for Ni-HT (I)a.

So it can be said that the increasing space time increased the selectivity of CO. When the selectivity values obtained for Ni-HT (II) is considered, it is obvious from the Fig. 32 that selectivity increased moderately between 300°C and 400°C and set to a constant value of about 1 over 400°C. Although the selectivity values of Ni-HT (II) is lower than the values of Ni-HT (I)b over 400°C, it is clear that Ni-HT (II) has approximately 5 times larger selectivity values than the Ni-HT (I)b has between 300°C and 400°C. So it can be concluded that as the Ni/Si ratio of catalyst increased the selectivity of CO increased between 300°C and 400°C. For each of the catalysts case, the CO selectivity did not change much at higher temperatures. These results together with hydrogen yield results indicated significant increase of catalyst activity at low temperatures by the increase of Ni/Si ratio of the catalyst.

During the reactions, cracking of C-C bonds actualized and CH₄ was formed as the temperature increased. The change of the selectivity of this side product with respect to temperature is presented in Figure 33.

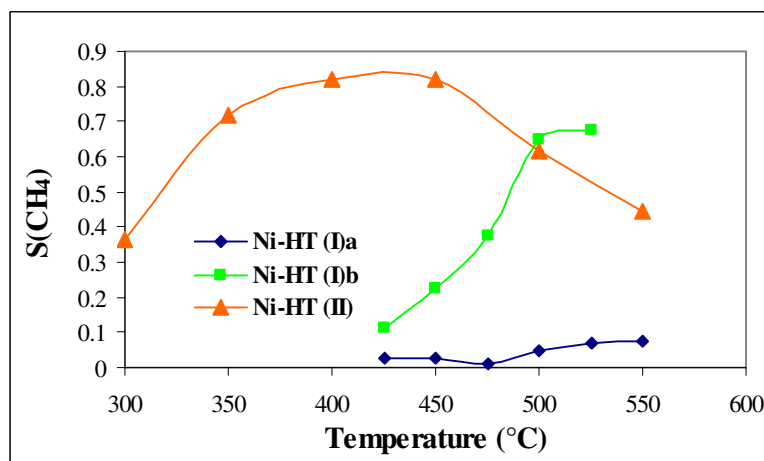


Figure 33 The variation of CH₄ selectivity with temperature

From the Fig. 33., it was observed that the methane selectivity reached to a maximum value of 0.07 (almost zero) for Ni-HT (I)a and 0.68 for Ni-HT (I)b over 500°C. As stated in the previous discussions, the activity of Ni-HT (I)a was lower than the activity of Ni-HT (I)b so lower selectivity of the products formed by Ni-HT (I)a is inevitable. When the selectivity of methane is considered for Ni-HT (II), the situation is somewhat different that the selectivity of CH₄ increased with increasing temperature up to 400°C reached to a maximum value of 0.81 and then decreased as the temperature increased over 400°C. When the selectivity trend of CH₄ for Ni-HT (I)b and Ni-HT (II) are compared, it is obvious that Ni-HT (II) has much higher selectivity values than Ni-HT (I)b has. So one can conclude that the increase in Ni/Si ratio in the catalyst resulted an increase in methane selectivity.

In addition to methane, some formaldehyde was formed as a side product. The variation of the selectivity of formaldehyde with temperature was plotted as in the Figure 34. In this case considering the yield of formaldehyde is also meaningful. The general definition of yield is given in Eqn (7) and the formaldehyde yield values calculated from Eqn. (7) tabulated in Table 8.

$$\text{Yield of A} = \text{Conversion of ethanol} * \text{Selectivity of A} \quad (7)$$

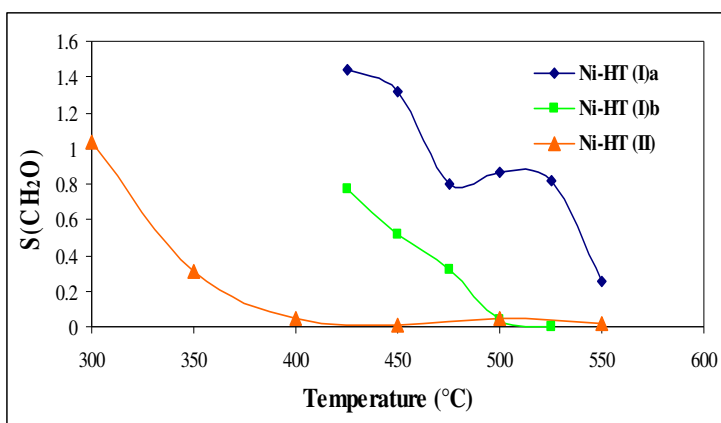
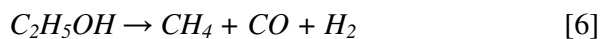


Figure 34 The variation of formaldehyde selectivity with temperature

Table 8. The variation of Formaldehyde yield with temperature

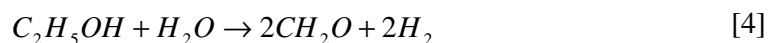
Temperature (°C)	Ni-HT (Ia)	Ni-HT (Ib)	Ni-HT (II)
	$Y_{\text{CH}_2\text{O}}$	$Y_{\text{CH}_2\text{O}}$	$Y_{\text{CH}_2\text{O}}$
300	-	-	0.02
350	-	-	0.05
400	-	-	0.02
425	0.04	0.07	-
450	0.05	0.09	0.01
475	0.11	0.11	-
500	0.09	0.13	0.04
525	0.11	0.18	-
550	0.19	0.03	0.02

As methane was formed, the formation of some formaldehyde was expected (Rxn [2]) as a result of cracking reaction. However at Figure 34, a sharp decrease of formaldehyde selectivity was observed with an increase in temperature where the methane selectivity was increasing, indicating further decomposition (or reforming) of formed formaldehyde to CO and H₂ (Rxn [3]). According to the steam reforming reaction given as Rxn [1], moles of hydrogen produced per mole of ethanol reacted should be four. However in our case this ratio was about 1.7 at high temperatures for Ni-HT (I)b and 2.1 for Ni-HT (II). On the other hand, according to the summation of Rxn [2] and Rxn [3] (giving Rxn. [6]) one mole of hydrogen was expected to form from one mole of ethanol.



Our results showed that steam reforming reaction (Rxn [1]) and the ethanol decomposition reactions (Rxn. [2] and [3]) take place in parallel at high

temperatures. Moreover, it is understood from the Fig.34 that the main carbon containing side product was formaldehyde at lower temperatures. Quite high formaldehyde selectivities were observed at temperatures lower than 450°C and especially for Ni-HT (I)a . With an increase of space time, further decomposition of formaldehyde is expected. At such low temperatures formation of methane is quite low (Figure 33), indicating the insignificance of the cracking reaction of ethanol especially at low temperatures and low space times. Formation of significant amount of formaldehyde at such low temperatures without formation of methane indicated the occurrence of Reaction [4].



When the selectivity of formaldehyde for Ni-HT (II) is compared to that of Ni-HT (I)b, it can be said that selectivity values of Ni-HT (I)b is much higher than that of Ni-HT (II) at the same temperatures. So it can be concluded that increasing Ni/Si ratio decreased the selectivity of formaldehyde.

In the Figure 35, the selectivity of CO₂ for Ni-HT (I)a and Ni-HT (I)b were plotted together in (A) whereas the CO₂ selectivity values for Ni-HT (II) was plotted separately in (B). The reason of giving two different plots came from the selectivity values of Ni-HT (II) being much greater than the values of Ni-HT (I)a and Ni-HT (I)b. So plotting three of the profiles in one curve resulted indistinct profiles for Ni-HT (I)a and Ni-HT (II).

From Fig. 35, it is clear that the selectivity of CO₂ increased as the temperature increased for each of the three cases. When Fig.35.(A) was considered, it was observed that Ni-HT (I)b with higher space time had higher selectivity values than the Ni-HT (I)a had meaning that higher space time resulted in higher CO₂ selectivity. It should be noted that the only trace amounts of CO₂ was observed in the system this indicated the negligible contribution of the water gas shift reaction in this system. When the Fig. 35.(B) was considered, Ni-HT (II) gave higher CO₂ selectivity values than the remaining two catalysts did. It reached to a maximum value of 0.53 at 550°C.

So it can be concluded that increasing Ni/Si ratio in the Ni-MCM-41 catalysts, resulted in higher selectivity toward CO₂.

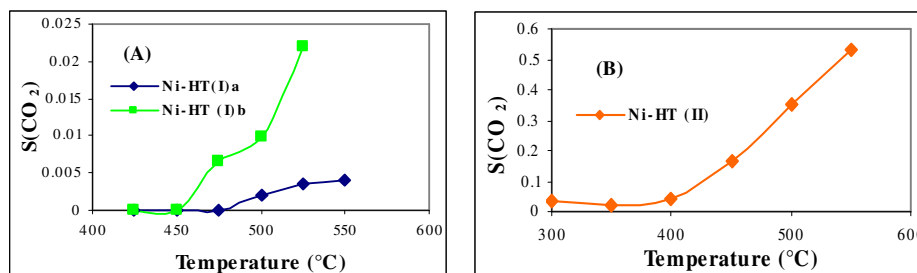


Figure 35. The selectivity of CO₂ (A) for Ni-HT (I)a and Ni-HT (I)b (B) for Ni-HT (II)

Of course, number of intermediate steps may be involved in such a reforming reaction. Another product observed at lower temperatures and especially at small residence times (Ni-HT (I)a) and also at higher Ni/Si ratios at high temperatures (Ni-HT (II)) is ethylene, indicating the occurrence of the dehydration reaction of ethanol (Rxn. [5]), together with steam reforming reactions (Rxn. [1] and [4]). A typical set of selectivity values of the products obtained at for Ni-HT (I)a, Ni-HT (I)b and Ni-HT (II) are listed in Table 9.

When the selectivity of Ni-HT (I)a and Ni-HT (I)b were considered, it was noticed that at higher space times, ethylene selectivity was much lower, indicating further decomposition and/or reforming of formed ethylene (Table 9). On the other hand, the selectivity values of ethylene for Ni-HT (II) is lower at the 400°C and higher at the 450-550°C than the selectivity values of ethylene for Ni-HT (I)b. So, increase in the Ni/Si ratio increased the dehydration reaction so as the selectivity of the ethylene. Formation of some ethylene in the experiments is an indication of presence of some acid sites in the Ni-MCM-41 catalyst synthesized in this work. In fact MCM-41 is not highly acidic [66].

Table 9. Ethylene selectivity data for Ni-HT (I)aa, Ni-HT (I)b and Ni-HT (II)

Temperature (°C)	Ni-HT (I)a	Ni-HT (I)b	Ni-HT (II)
	S _{C₂H₄}	S _{C₂H₄}	S _{C₂H₄}
400	0.19	0.04	0.02
425	0.05	0.02	-
450	0.05	0	0.01
475	0	0	-
500	0	0	0.02
550	0	0	0.02

In the literature [18], formation of some acetaldehyde was also indicated in the steam reforming of ethanol over Co based catalysts. However in this study no acetaldehyde was observed when Cu and Ni based MCM-41 were used.

In the experiments, some carbon deposition was observed at temperatures higher than 500°C. Much higher coke formation at lower temperatures would be expected with more acidic catalytic materials.

5.2.ii. Catalytic Activity of Copper Based MCM-41 type catalysts

The reactions performed at atmospheric pressure and the conditions given in Table 7 for Cu-HT (I) and Cu-Imp (II) gave main products of ethylene (C₂H₄) and formaldehyde (CH₂O) and unlike nickel based MCM-41 catalysts, these two copper based MCM-41 catalysts did not show good activity for steam reforming of ethanol to give hydrogen. Some other products like carbon dioxide (CO₂), carbon monoxide (CO) and methane (CH₄) also formed during reactions.

When the products formed during reactions were considered the possible reaction sequence appeared to be similar to the one given for nickel based catalysts in Section 5.1.i as Rxn. [1-7]. However in this case, the

catalysts were mainly selective to the dehydration reaction giving ethylene (Rxn [5]) and the formation of formaldehyde (Rxn [4])

In this section the results of Cu-HT (I) synthesized by high temperature direct synthesis method and Cu-Imp (II) synthesized by impregnation method will be dealt in order to analyze the effect of the preparation technique to the activity of the catalyst.

5.2.ii.a. Conversion of Ethanol

The conversion values of ethanol for Cu-Imp (II) and Cu-HT (I) were calculated by Equation (4) and the variation of these values with temperature is given in Figure 36.

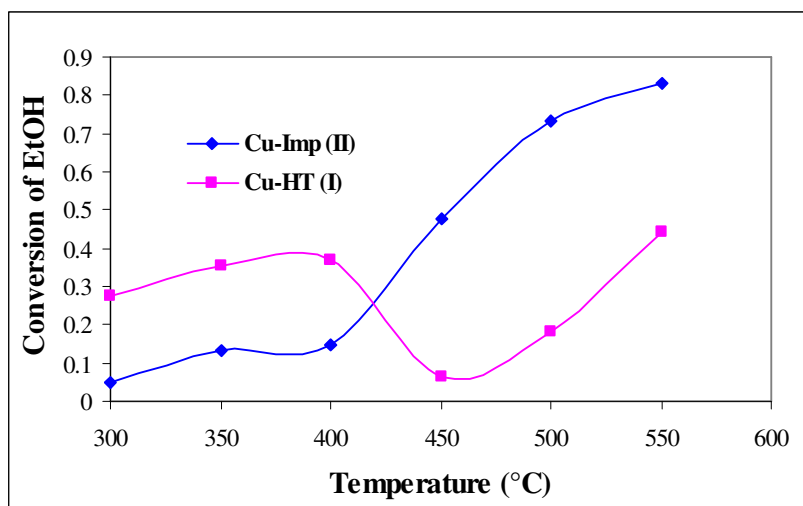


Figure 36. Variation of conversion of ethanol with temperature

As it is seen from Fig.36, the conversion of ethanol increased with an increase in the temperature and reached to a maximum value of 0.83 over 500°C during the reactions performed by Cu-Imp (II) catalyst. However, the situation for Cu-HT (I) is somewhat different. The conversion increased to a value of 0.36 at 400°C but then fell to a value of 0.066 and kept increasing. It

has finally reached to a maximum value of 0.44. Some coke formation over 400°C might be a possible factor in this decrease of conversion. It can be understood from Figure 36, the sample prepared by impregnation method showed more activity than the sample prepared by high temperature direct synthesis method.

5.2.ii.b. Yield of hydrogen

The yield of hydrogen values for Cu-HT (I) and Cu-Imp (II) catalysts were found by using Eqn. (5) and plotted in Figure 37 with respect to temperature.

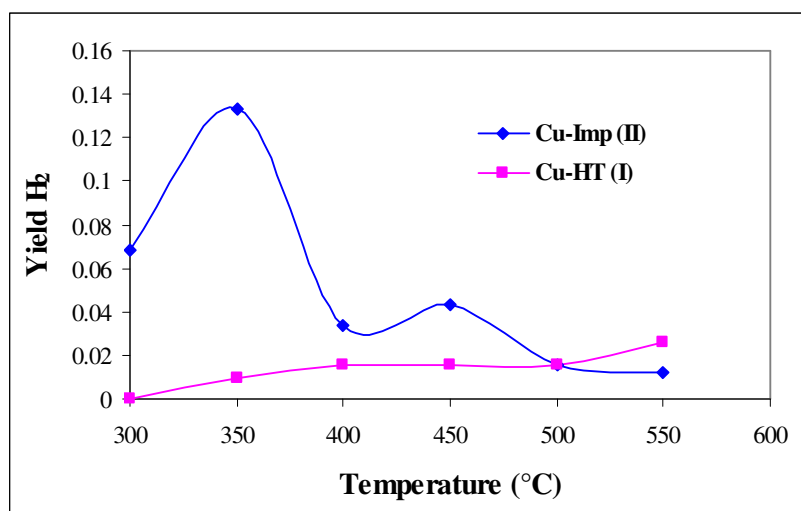


Figure 37. Variation of hydrogen yield with temperature

The hydrogen yield spectra given in Figure 37 showed that Cu-Imp (I) produced hydrogen at higher yields (maximum value about 0.14 at 350°C) than the Cu-HT (I) did (maximum value about 0.04 at 550°C). Moreover, hydrogen yield curve of Cu-Imp (II) showed decreasing trend with increasing

temperature where as the opposite is valid for the Cu-HT (I). The major conclusion from these results is that the hydrogen yield values were very low, indicating that these catalysts were not active for the steam reforming of ethanol.

5.2.ii.c. Selectivity of Side Products

Ethylene and formaldehyde were observed as main products of the reactions catalyzed by copper based catalysts. The selectivity of each product was calculated by Eqn. (6).

The variation of selectivity of ethylene with temperature was presented in the Fig. 38.

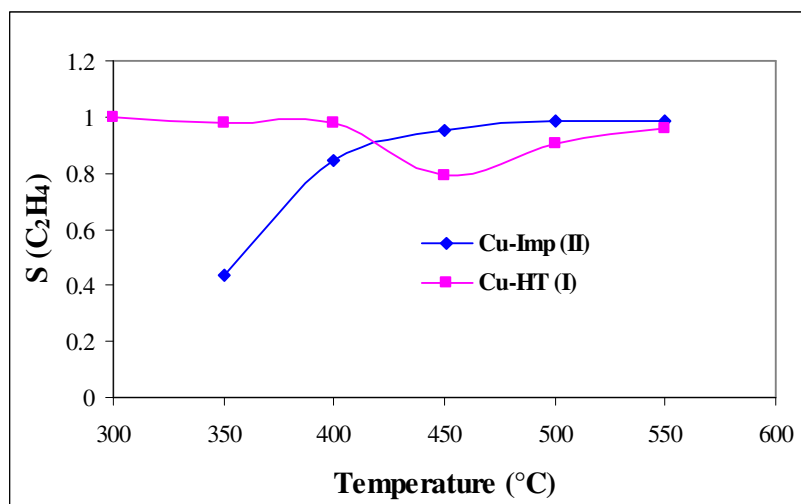


Figure 38. The variation of selectivity of ethylene with temperature

In both of the catalyst cases the selectivity of ethylene had a maximum value of 1 (Fig. 38). However, it was observed that while the selectivity of Cu-Imp (I) increased with increasing temperature and reaching to 1 at 550°C, the

selectivity of ethylene values of Cu-HT (I) did not change too much and was maximum value of 1 at most of the temperatures.

The yield values of ethylene for copper based catalysts, are also significant to mention. So the variation of ethylene yield with temperature is given in Fig.39.

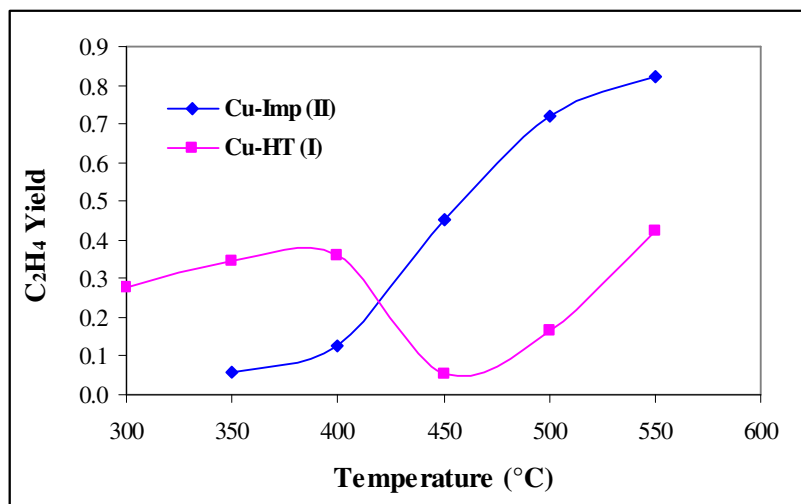


Figure 39. The variation of ethylene yield with temperature

An interesting result is that with Cu-Imp (II) catalyst an ethylene yield value more than 0.8 was achieved at about 550°C (Fig. 39). Copper impregnated catalysts were found to be quite good catalysts for ethanol dehydration, over 450°C

Formaldehyde can also be considered as one of the major products of the reactions catalyzed by copper based MCM-41 catalysts. The change of the selectivity of formaldehyde with temperature is given in Figure 40.

As in the Ni-MCM-41 catalysts' case the selectivity of formaldehyde has diminished from maximum value of about 1.9 at 300°C with increasing

temperature for Cu-Imp (II) (Fig. 40). The decrease of formaldehyde is due to the cracking of formaldehyde at higher temperatures. For Cu-HT (I), however, the selectivity did not change too much between 300°C and 400°C. Then the selectivity of formaldehyde decreased simultaneously by increasing temperature similar to the situation of Cu-Imp (II). However, since ethanol conversion values are quite low below 400°C, formaldehyde yield values were also quite low. Formaldehyde yield values were much lower than 0.1 in these experiments.

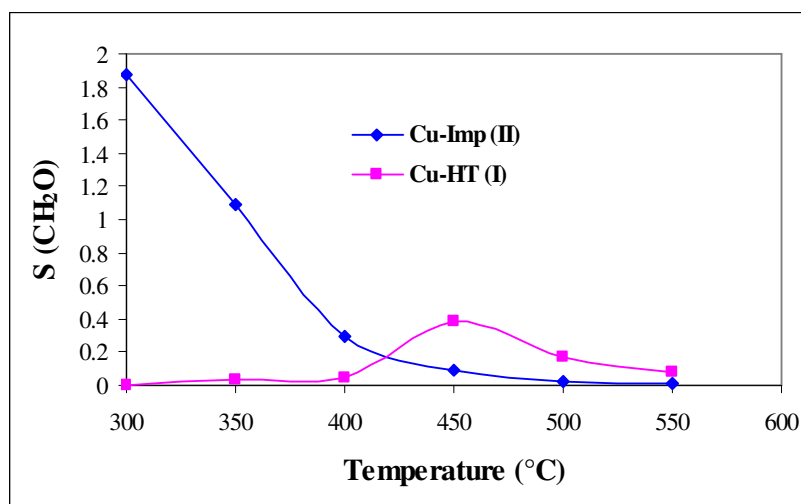


Figure 40. The change of selectivity of formaldehyde with temperature

The next table, Table 10, gives the variation of the selectivity of CO with temperature.

Table 10. The change of selectivity of CO with temperature

Temperature (°C)	Cu-HT (I)	Cu-Imp (II)
	S_{CO}	S_{CO}
300	0	0.013
350	0.001	0.007
400	0.001	0.002
450	0.014	0.002
500	0.010	0.002
550	0.004	0.003

The selectivity of CO has decreased from a maximum value of 0.013 at 300°C to a minimum value of 0.002 at 450°C and then did not change so much by increasing temperature for Cu-Imp (II). On the other hand, selectivity values got higher by increasing temperature up to 450°C reaching to 0.014 at 450°C then decreased between 450°C and 550°C by increasing temperature.

Very small amount of methane was also formed during the reactions catalyzed by Cu-HT (I) and Cu-Imp (II). The selectivity of methane was tabulated against temperature in Table 11.

Table 11. The variation of selectivity of methane with temperature

Temperature (°C)	Cu-HT (I)	Cu-Imp (II)
	S_{CH_4}	S_{CH_4}
300	0	0.013
350	0.001	0.010
400	0.001	0.003
450	0.009	0.002
500	0.004	0.002
550	0.002	0.003

As it can be understood from Table 11, the selectivity of CH₄, has decreased by increasing temperature for the reactions performed by Cu-Imp (II). The maximum value was reached was 0.013 at 300°C. For the Cu-Imp (II) catalyzed reactions, the selectivity values obtained were not as high as the values of Cu-Imp (II). The selectivity of CH₄ increased with an increase in temperature up to 450°C and reached to 0.009 at 450°C. However from 450°C point to 550°C, selectivity of CH₄ has gradually decreased with increasing temperature.

The behavior of the selectivity of CO₂ with respect to temperature was also given in Table 12.

Table 12. The variation of selectivity of CO₂ with temperature

Temperature (°C)	Cu-HT (I)	Cu-Imp (II)
	S_{CO_2}	S_{CO_2}
300	0	0.098
350	0.0004	0.017
400	0.0004	0.001
450	0.0040	0.003
500	0.0027	0.001
550	0.0014	0.001

It was observed from Table 12 that the selectivity of CO₂ has decreased by increasing temperature from 0.1 at 300°C to almost zero over 350°C during the reactions catalyzed by Cu-Imp (II). However, lower selectivity values (maximum 0.004, at 450°C) were obtained for the reactions done by Cu-HT (I). In addition, the selectivity of CO₂ did not change by changing temperature.

CONCLUSIONS & RECOMMENDATIONS

In this study, the steam reforming of ethanol for hydrogen production via Ni-MCM-41 and Cu-MCM-41 catalysts were examined. For this reason two Ni-MCM-41 catalysts prepared by high temperature direct synthesis method having different Ni/Si ratios and two Cu-MCM-41 catalysts having same Cu/Si ratio but prepared by different methods namely; high temperature direct synthesis method and impregnation were used in the reforming reaction of ethanol and the following remarks were concluded;

- Nickel and copper incorporated MCM-41 type catalytic materials were successfully synthesized using one pot direct hydrothermal procedure.
- Ni-MCM-41 synthesized by high temperature direct synthesis method had typical MCM-41 structure. The d_{100} and lattice parameter values of Ni-HT (I) (Ni-MCM-41 sample having 0.036 Ni/Si atomic ratio) was obtained as 3.96 and 4.57 nm., respectively where as d_{100} and lattice parameter values of Ni-HT (II) (Ni-MCM-41 sample having 0.15 Ni/Si atomic ratio) was 3.45 and 3.98 nm. In addition Ni-HT (I) was found to have a surface area of 860.5 m²/g and 2.7 nm pore diameter while the surface area and pore diameter of Ni-HT (II) were 944.9 m²/g and 2.6 nm respectively.
- The d_{100} and lattice parameter values for a typical Cu-MCM-41 prepared by impregnation method having Cu/Si atomic ratio of 0.19 were obtained as 3.6 and 4.2 nm., respectively. This sample also has a 631 m²/g surface area and 2.5 nm pore diameter. Cu-HT (I) sample (prepared by high temperature direct synthesis method) found out to

have d_{100} and lattice parameter values of 3.32 and 3.83 nm. In addition, this sample had a 950.1 m²/g surface area and 3.2 nm pore diameter

- Nickel incorporated MCM-41 type materials showed high activity in the steam reforming of ethanol at temperatures lower than 500°C. Ni-HT (I) sample (having Ni/Si ratio of 0.036) were tested at two different space times; 0.024 s.g/ml (Ni-HT (I)a) and 0.068 s.g/ml (Ni-HT (I)b) in order to see the effect of space time on the reaction. It was observed that over 500°C almost complete conversion with a hydrogen yield value of 1.7 was achieved Ni-HT (I)b. It was understood that increasing space time both increased the conversion of ethanol and yield of hydrogen.
- The activities of Ni-HT (I) and Ni-HT (II) samples were compared in order to understand the impact of Ni/Si ratio of catalyst on the steam reforming reaction. It can be said that Ni-HT (II) (having higher Ni/Si ratio) showed much higher activity at steam reforming of ethanol. Since the conversion of ethanol and yield of hydrogen were higher quantitatively for the sample having higher Ni/Si ratio.
- Copper incorporated MCM-41 type materials showed poor activity in steam reforming of ethanol to produce hydrogen. However, these catalysts showed quiet high activity in ethanol dehydration to produce ethylene. Cu-HT (I) and Cu-Imp (II) were considered together in order to see the effect of the preparation method. Cu-HT (I) had an ethanol conversion value of 0.5 where as Cu-Imp (II) had an ethanol conversion value of 0.83. So it was concluded that the Cu-MCM-41 sample prepared by impregnation method showed better activity than the sample prepared by high temperature direct synthesis method.
- From overall product distribution, the main reaction mechanism composed of steam reforming of ethanol, ethanol cracking, dehydration forming ethylene, formaldehyde formation, formaldehyde cracking and

steam reforming of formaldehyde and coke formation reaction steps. The formaldehyde formation and dehydration reactions mainly occurred at lower temperatures where as they decomposed into other products at higher temperatures. The main products were H₂, CO, CO₂, CH₄, CH₂O and C₂H₄.

From all these conclusions for future studies it is recommended that the effect of EtOH/H₂O feed ratio should be tested. In order to increase activity, coke formation should be prevented and this can be done by supplying oxygen to the reaction medium. From the reaction results, it was also understood that the increasing Ni/Si ratio in Ni-MCM-41 resulted higher activity in steam reforming of ethanol. So the future studies should also include the usage of the Ni-MCM-41 having higher Ni/Si ratio in the steam reforming reaction. In addition, Ni-MCM-41 samples prepared by impregnation should also be employed in the steam reforming reaction. Different reactors such as microwave reactors can be tested in order to save energy. Finally the catalysts can be improved by incorporating more than one active metals meaning preparing bi metallic catalysts. From the literature survey these bimetallic catalysts can be Co/Ni-MCM-41, Rh/Ni-MCM-41, Rb/Ni-MCM-41. These recommendations may improve the steam reforming reaction results and may yield higher H₂. Copper incorporated MCM-41 is not recommended for steam reforming reaction of ethanol to produce hydrogen. However, this catalyst showed high yield of ethylene which is the feedstock of petrochemistry.

REFERENCES

- [1] Wikipedia the Free Encyclopedia, http://en.wikipedia.org/wiki/Main_Page, http://en.wikipedia.org/wiki/Energy_density, Last access date: June, 2007
- [2] Das, D., Veziroglu, T. N., Hydrogen Production by Biological Processes: A Survey of Literature. *Int. J. Hydrogen Energy*, 2001, 26, 13-28.
- [3] Stanford Formal Reasoning Group, <http://www.formal.stanford.edu>, html, <http://www.formal.stanford.edu/jmc/progress/hydrogen.html>, Last access date: June, 2007
- [4] Yahoo Geocities, <http://geocities.yahoo.com>, http://www.geocities.com/aardduck/fc_storage.html, Last access date: June 2007
- [5] Huber, G. W., Shabaker, J. W., Dumesic, J. A. Raney, Ni-Sn Catalyst for H₂ Production from Biomass-Derived Hydrocarbons, *Science*, 2003, 300, 2075
- [6] Kawatsu, S., Advanced PEFC development for fuel cell powered vehicles, *Journal of Power Sources* , 1998, 71, 150-155
- [7] Panik, F., Fuel cells for vehicle applications in cars - bringing the future closer, *Journal of power sources*, 1998, 71, 36-38
- [8] Klouz, V., Fierro, V., Denton, P., Katz, H., Lisse, J.P., Bouvot-Mauduit, S., Ethanol reforming for hydrogen production in a hybrid electric vehicle: process optimization, *J Power Sources*, 2002, 105, 26-34.

- [9] Marino, F., Boveri, M., Baronetti, G., Laborde, M., Hydrogen Production via Catalytic Gasification of Ethanol A Mechanism Proposal over Copper-Nickel Catalysts, *Int. J. Hydrogen Energy*, 2004, 29, 67-71.
- [10] Haryanto, A., Fernando, S., Murali, N., Adhikari, S., Current Status of Hydrogen Production Techniques by Steam Reforming of Ethanol A Review. *Energy & Fuels*, 2005, 19, 5, 2098-2196
- [11] Garcia E. Y., Laborde M. A., Hydrogen production by the steam reforming of ethanol: thermodynamic analysis, *Int. J. Hydrogen Energy*, 1991, 16, 307
- [12] Vasudeva K., Mitra N., Umasankar P., Dhingra S.C., Steam reforming of ethanol for hydrogen production: thermodynamic analysis, *Int. J. Hydrogen Energy*, 1996, 21, 13.
- [13] Fishtik I., Alexander A., Datta R., Geana D., A thermodynamic analysis of hydrogen production by steam reforming of ethanol via response reactions, *International Journal of Hydrogen Energy*, 2000, 25, 31-45
- [14] Ionnidides T., Thermodynamic analysis of ethanol processors for fuel cell applications, *Journal of Power Sources*, 2001, 92, 17-25
- [15] Llorca J., Piscina P.R., Sales J., Homs N., Direct production of hydrogen from ethanolic aqueous solutions over oxide catalysts, *Chem. Commun.*, 2001, 641-642
- [16] Haga, F., Nakajima, T., Miya, H., Mishima, S., Catalytic Properties of Supported Cobalt Catalysts for Steam Reforming of Ethanol, *Catal. Lett.*, 1997, 48, 223-227.

[17] Batista, M. S., Santos, R. K. S., Assaf, E. M., Assaf, J. M., Ticianelli, E. A., Characterization of the Activity and Stability of Supported Cobalt Catalysts for the Steam Reforming of Ethanol, *J. Power Sources*, 2003, 124 (1), 99-103.

[18] Llorca, J., Homs, N., Sales, J., De La Piscina, P. R., Efficient Production of Hydrogen over Supported Cobalt Catalysts from Ethanol Steam Reforming, *J. Catal.* 2002, 209 (2), 306-317.

[19] Aupretre, F., Descorme, C., Duprez, D., Bio-ethanol Catalytic Steam Reforming over Supported Metal Catalysts, *Catal. Commun.*, 2002, 3 (6), 263-267.

[20] Cavallaro, S., Ethanol Steam Reforming on Rh/Al₂O₃ Catalysts., *Energy Fuels* 2000, 14, 1195-1199.

[21] Freni, S., Rh-Based Catalysts for Indirect Internal Reforming Ethanol Applications in Molten Carbonate Fuel Cells., *J. Power Sources* 2001, 94 (1), 14-19.

[22] Cavallaro, S., Chiodo, V., Freni, S., Mondello, N., Frusteri, F. Performance of Rh/Al₂O₃ Catalyst in the Steam Reforming of Ethanol: H₂ Production for MC., *Appl. Catal., A* 2003, 249 (1), 119-128.

[23] Liguras, D. K., Kondarides, D. I., Verykios, X. E., Production of hydrogen for fuel cells by steam reforming of ethanol over supported noble metal catalysts., *Applied Catalysis B: Environmental*, 2003, 43, 345-54.

[24] Casanovas, A., Llorca, J., Homs, N., Fierro, J.L., De La Piscina, P. R., Ethanol reforming processes over ZnO-supported palladium catalysts: effect of alloy formation, *J Mol Catal A Chem.*, 2006, 250, 44-9.

- [25] Ni, M, Leung, Y. C. D, Leung, M. K. H., A review on reforming bio-ethanol for hydrogen production, *Int J Hydrogen Energy*, 2007, doi:10.1016/j.ijhydene.2007.04.038
- [26] Marino, F. J., Cerrella, E. G., Duhalde, S., Jobaggy, M., Laborde, M.A., Hydrogen from steam reforming of ethanol characterization and performance of copper-nickel supported catalysts, *Int. J. Hydrogen Energy*, 1998, 23(12), 1095
- [27] Marino, F., Boveri, M., Baronetti, G., Laborde, M., Hydrogen production from steam reforming of bioethanol using Cu/Ni/K/ γ -Al₂O₃ catalysts. Effect of Ni, *International Journal of Hydrogen Energy*, 2001, 26, 665–668
- [28] Marino, F., Boveri, M., Baronetti, G., Laborde, M., Hydrogen production via catalytic gasification of ethanol A mechanism proposal over copper–nickel catalysts, *International Journal of Hydrogen Energy*, 2004, 29, 67 – 71
- [29] Fatsikostas, A. N., Verykios, X.E., Reaction network of steam reforming of ethanol over Ni-based catalysts, *Journal of Catalysis*, 2004, 225, 439–452
- [30] Fierro, V., Akdim, O., Provendier, H., Mirodatos, C., Ethanol oxidative steam reforming over Ni-based catalysts, *Journal of Power Sources*, 2005, 145, 659–666
- [31] Akande, A., Production of Hydrogen by Reforming of Crude Ethanol, Master Thesis, University Saskatchewan, 2005
- [32] Freni, S., Cavallaro, S., Mondello, N., Spadaro, L., Frusteri, F., Steam reforming of ethanol on Ni/MgO catalysts: H₂ production for MCFC, *Journal of Power Sources*, 2002, 108, 53–57
- [33] Frusteria, F., Freni, S., Chiodo, V., Donato, S., Bonura, G., Cavallaro, S., Steam and auto-thermal reforming of bio-ethanol over MgO and CeO₂ Ni

supported catalysts, International Journal of Hydrogen Energy, 2006, 31, 2193
– 2199

[34] Yang, Y., Ma, J., Wu, F., Production of hydrogen by steam reforming of ethanol over a Ni/ZnO catalyst, Int. J. Hydrogen Energy, 2006, 31, 877-882.

[35] Cavallaro, S., Freni, S., Ethanol steam reforming in a molten carbonate fuel cell. A preliminary kinetic investigation, Int. J. Hydrogen Energy , 1996, 21, 6, 465.

[36] Nishiguchi, T., Matsumoto, T., Kanai, H., Utani, K., Matsumura, Y., Shen, W. J., Imamura, S., Appl. Catal. A: Gen., 2005, 279, 273

[37] Amphlett, J. C., Leclerc, S., Mann, R. F., Peppley, B. A., Roberge, P. R., Fuel Cell Hydrogen Production By Catalytic Ethanol-Steam Reforming, Proc. 33rd Intersoc. Energy Conserv. Eng. Conf. (cf CA), 1998, 129, 205166.

[38] Duan, S., Senkan, S., Catalytic Conversion of Ethanol to Hydrogen Using Combinatorial Methods. Ind. Eng. Chem. Res. 2005, 44, 6381-6386

[39] Carrero, A., Calles, J.A, Vizcaino, A.J., Hydrogen production by ethanol steam reforming over Cu-Ni/SBA-15 supported catalysts prepared by direct synthesis and impregnation, Applied Catal.,

[40] Rouquerol, J., Avnir, D., Fairbridge, C.W., Everett, D.H., Haynes, J.H., Pernicone, N., Ramsay, J.D.F., Sing, K.S.W., Unger, K.K., Recommendations for the characterization of porous solids, Pure & Appl. Chem., 1994, 66, 1739-1758

[41] Øye, G., Sjoblom, J., Stocker, M., Synthesis, characterization and potential applications of new materials in the mesoporous range, Advances in Colloid and Interface Science, 2001, 89-90, 439-466

[42] Kresge, C.T., Leonowicz, M. E., Roth, W. J., Vartuli, J. C., Beck, J. S., A new family of mesoporous molecular sieves, *Nature*, 1992, 359, 710

[43] Myers, D., *Surfactant Science and Technology*, 2nd ed., 1992, 28, 7, 936

[44] Lawrence, M. J., *Surfactant Systems: Their Use in Drug Delivery*, *Chem. Soc. Rev.* 1994, 23, 417-424.

[45] Behrens, P., Glaue, A., Haggemüller, C., Schechner, G., Structure-directed materials syntheses: Synthesis field diagrams for the preparation of mesostructured silicas, *Solid State Ionic* 1997, 101-103, 255-260

[46] Library of Universitat Utrecht, <http://www.library.uu.nl>, <http://www.library.uu.nl/digiarchief/dip/diss/2003-0325-14324/inhoud.htm>, April, 2007

[47] Vartuli, J. C., Schmitt, K. D., Kresge, C. T., Roth, W. J., Leonowicz, M. E., McCullen, S. B., Hellring, S. D., Beck, J. S., Schlenker, J. L., Olson, D. H.; Sheppard, E. W. Effects of Surfactant/Silica Molar Ratios on the Formation of Mesoporous Molecular Sieves: Inorganic Mimicry of Surfactant Liquid-Crystal Phases and Mechanistic Implications. *Chem. Mater.* 1994, 6, 2317-2326.

[48] Xiu S., Zhao, G. Q., Lu, M., Millar, G. J., *Advances in Mesoporous Molecular Sieve MCM-41* *Ind. Eng. Chem. Res.*, 1996, 35, 2075-2090

[49] Monnier, A., Schuth, F., Huo, Q., Kumar, D., Margolese, D., Maxwell, R. S., Stucky, G. D., Krishnamurthy, M., Petroff, P., Firouzi, A., Janicke, M., Chmelka, B. F., Cooperative Formation of Inorganic-Organic Interfaces in the Synthesis of Silicate Mesostructures, *Science*, 1993, 261, 1299-1303.

- [50] Anderson, M. W., Simplified Description of MCM-48 Zeolites, 1997, 19, 220-227
- [51] Schumacher, K., Grun, M., Unger, K. K., Novel synthesis of spherical MCM-48, *Microporous and Mesoporous Materials*, 1999, 27, 201–206
- [52] Vartuli, J.C., Malek, A., Roth, W.J., Kresge, C.T., McCullen, S. B., The sorption properties of as-synthesized and calcined MCM-41 and MCM-48, *Microporous and Mesoporous Materials*, 2001, 44-45, 691-695.
- [53] Huo, Q., Margolese, D. I., Stucky, G. D., Surfactant Control of Phases in the Synthesis of Mesoporous Silica-Based Materials, *Chem. Mater.* 1996, 8, 1147
- [54] Roth, W. J., Synthesis of the Cubic Mesoporous Molecular Sieve MCM-48, 2000, US Patent No. 6, 096, 288
- [55] Yao, N., Synthesis and Characterization of Pt/Sn-MCM-41 Petroleum Reforming Catalysts, PhD Thesis, Yale University, January 2002.
- [56] Wikipedia the Free Encyclopedia, http://en.wikipedia.org/wiki/Main_Page, http://en.wikipedia.org/wiki/Scanning_electron_microscope#Scanning_process, Last Access date: June, 2007
- [57] Velu, S., Wang, L., Okazaki, M., Suzuki, K., Tomura, S., Characterization of MCM-41 mesoporous molecular sieves containing copper and zinc and their catalytic performance in the selective oxidation of alcohols to aldehydes, *Microporous and Mesoporous Materials*, 2002, 54, 113–126
- [58] Guo, X., Lai, M., Kong, Y., Ding, W., Yan, Q., Novel Coassembly Route to Cu-SiO₂ MCM-41-like Mesoporous Materials, *Langmuir*, 2004, 20, 2879-2882

[59] Wan, Y., Ma, J., Wang, Z., Zhou, W., Kaliaguine, S., Selective Catalytic Reduction of NO over Cu-Al-MCM-41, *Journal of Catalysis*, 2004, 227, pp. 242-252

[60] Noreña-Franco, L., Hernandez-Perez, I., Aguilar-Pliego, J., Maubert-Franco, A., Selective hydroxylation of phenol employing Cu-MCM-41 catalysts, *Catalysis Today*, 2002, 75, 189–195

[61] Wojcieszak, R., Monteverdi, S., Mercy, M., Nowaka, I., Ziolk, M., Bettahar, M. M., Nickel containing MCM-41 and AlMCM-41 mesoporous molecular sieves Characteristics and activity in the hydrogenation of benzene, *Applied Catalysis A: General*, 2004, 268, 241–253

[62] Du, G., Lim, S., Yang, Y., Wang, C., Pfefferle, L., Haller, G. L., Methanation of carbon dioxide on Ni-incorporated MCM-41 catalysts: The influence of catalyst pretreatment and study of steady-state reaction, *Journal of Catalysis*, 2007, 249, 368-377

[63] Li, X., Wang, A., Zhang, S., Chen, Y., Hu, Y., Effect of surface Na⁺ or K⁺ ion exchange on hydrodesulfurization performance of MCM-41-supported Ni-W catalysts, *Applied Catalysis A: General*, 2007, 316, 134–141

[64] Nalbant , A., Doğu, T., Balcı, S ., Synthesis and characterization of Cu-MCM-41 type catalytic materials, *Micro-and Mesoporous Mineral Phases*, 2004, p. 259-260

[65] Sener, C., Dogu, T., Dogu, G., Effects of synthesis conditions on the structure of Pd incorporated MCM-41 type mesoporous nanocomposite catalytic materials with high Pd/Si ratios, *Microporous Mesoporous Materials*, 2006, 94, 89.

[66] Gucbilmez, Y., Dogu, T., Balci, S., Ethylene and acetaldehyde production by selective oxidation of ethanol using mesoporous V-MCM-41 catalyst, *Ind. Eng. Chem. Res.*, 2006, 45, 3496.

[67] Earth Science Educational Report Center,
<http://www.eserc.stonybrook.edu>,
<http://www.eserc.stonybrook.edu/ProjectJava/Bragg/>), Last Access
date:August, 2007

[68] PANalytical, <http://www.panalytical.com>,
<http://www.panalytical.com/index.cfm?pid=314>, Last Access date:August,
2007

[69] Sener, C., Synthesis and Characterization of Pd-MCM-Type Mesoporous Nanocomposite Materials, Master Thesis, METU, 2007

APPENDIX A.1. EDS

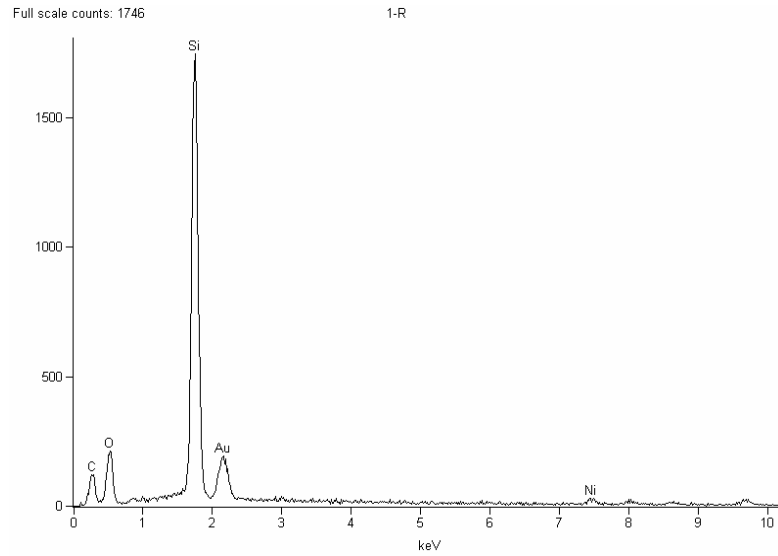


Figure 41. EDS of Ni-HT (I)

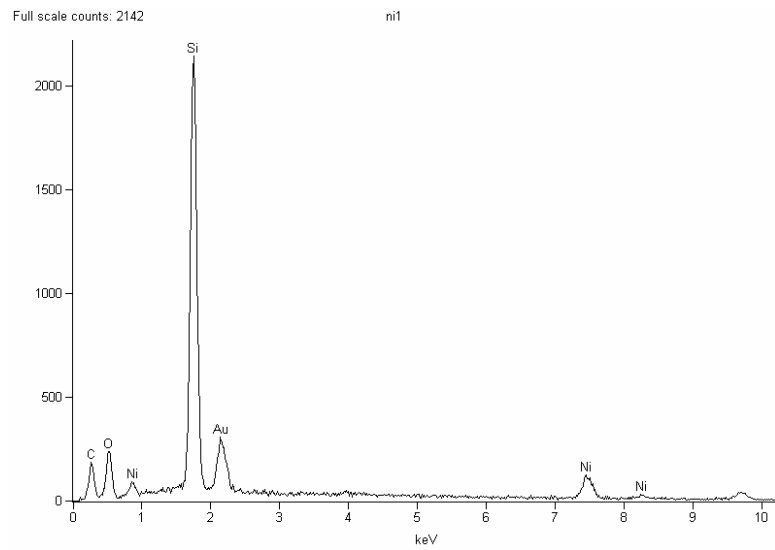


Figure 42. EDS of Ni-HT (II)

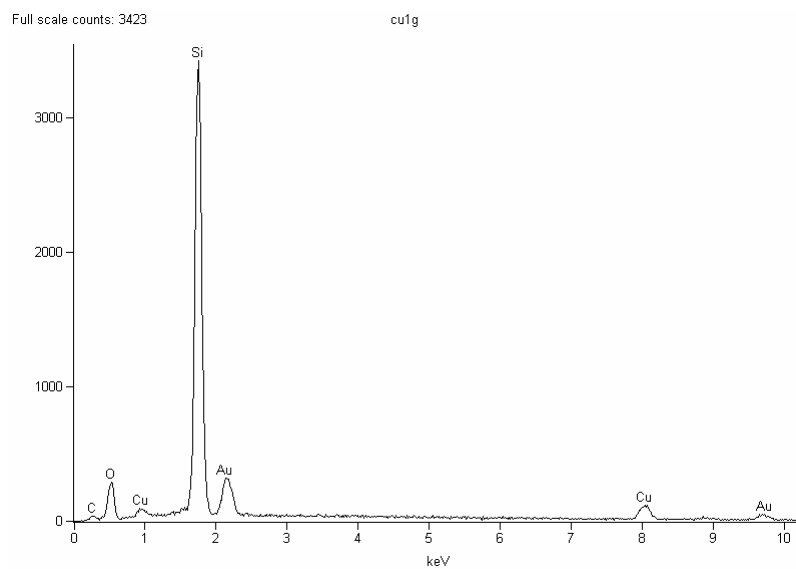


Figure 43. EDS of Cu-HT (I)

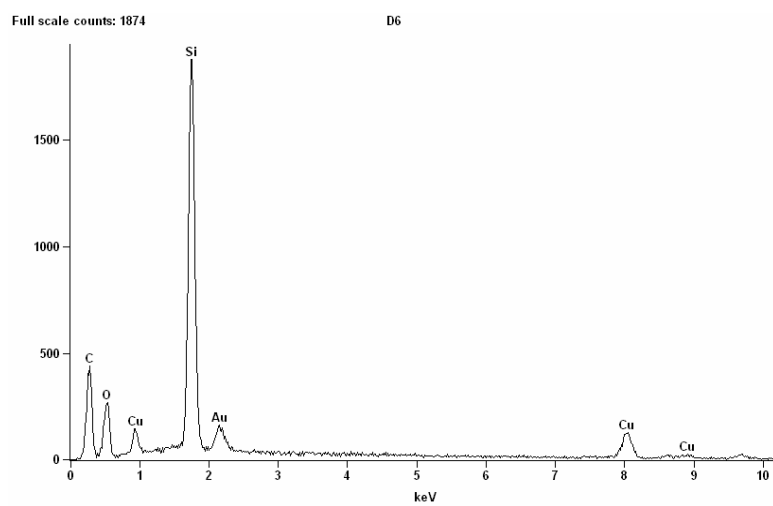


Figure 44. EDS of Cu-Imp (II) [59]

APPENDIX A.2. SEM

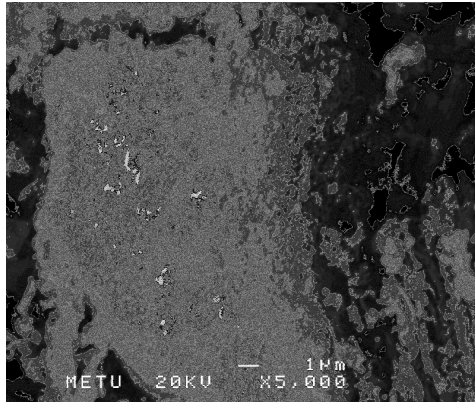


Figure 45. SEM image of Ni-HT (I)

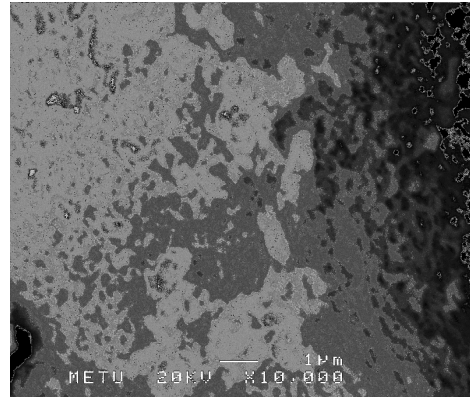


Figure 46. SEM image of Ni-HT (I)

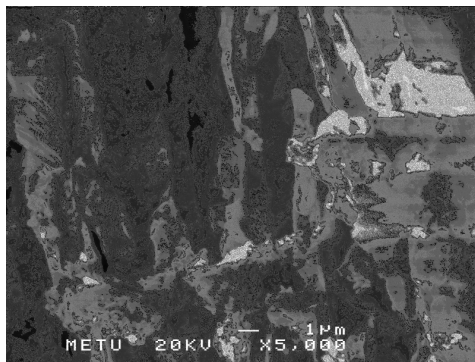


Figure 47. SEM image of Cu-HT (I)

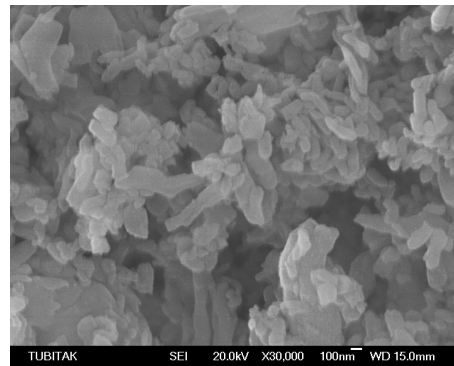


Figure 48. SEM image of Cu-Imp (II) [59]

APPENDIX B.1. Raw Reaction Data

Table 13. Raw Data Of Ni-HT (I)a

Ni-HT (I)a			
T=350 C			
peak #	Element	Area	Mole
1	H ₂	64.9	485.1275
	CO		116.55
2	H ₂	166.7	477.2621
3	H ₂ O +CO	643098	-
4	C ₂ H ₅ OH	176295	176295
	H ₂ O	643093.88	514475.11
peak #	Element	Area	Mole
1	H ₂	53.7	401.4075
	CO		522
2	H ₂	123	352.149
3	H ₂ O +CO	508778	-
4	C ₂ H ₅ OH	165929.9	165929.9
	H ₂ O	508759.55	407007.64
T=400 C			
peak #	Element	Area	Mole
1	H ₂	266.6	1992.835
	CO		1592.55
2	H ₂	645.7	1848.6391
3	CH ₄	263.7	1534.734
4	C ₂ H ₄	97.3	1050.84
5	H ₂ O +CO	546362.4	
6	CH ₂ O	630.6	3720.54
7	C ₂ H ₅ OH	164137.3	180551.03
	H ₂ O	546306.13	437044.9
T= 425 C			
1	H ₂	538.8	4027.53

Table 13 (Cont.d)

	CO		795
2	CH ₄	9.07	135.143
3	H ₂	1390	3979.57
4	CH ₄	274.5	1597.59
5	C ₂ H ₄	22.8	246.24
6	H ₂ O +CO	541372.1	
7	CH ₂ O	1247.6	7360.84
8	C ₂ H ₅ OH	151793	151793
	H ₂ O	541344.01	433075.21
T=450 C			
peak #	Element	Area	Mole
1	H ₂	916.8	6853.08
	CO		5333.25
2	CH ₄	19.4	289.06
3	H ₂	2225.5	6371.6065
4	CH ₄	282	1641.24
5	C ₂ H ₄	47.9	517.32
6	H ₂ O +CO	467836.1	
7	CH ₂ O	2105.9	12424.81
8	C ₂ H ₅ OH	111858.7	111858.7
	H ₂ O	467647.65	374118.12
T=475 C			
peak #	Element	Area	Mole
1	H ₂	1685.8	12601.355
	CO		19178.1
2	CH ₄	20.8	309.92
3	H ₂	3763.4	10774.614
4	H ₂ O +CO	466766.1	
5	CH ₂ O	1926.2	11364.58
6	C ₂ H ₅ OH	115448.2	115448.2
	H ₂ O	466088.43	372870.74
peak #	Element	Area	Mole
1	H ₂	1608.7	12025.033
	CO		14592.6
2	CH ₄	10	149

Table 13 (Cont.d)

3	H ₂	3721.4	10654.368
4	C ₂ H ₄	26.4	285.12
5	H ₂ O +CO	438630.2	
6	CH ₂ O	2036.6	12015.94
7	C ₂ H ₅ OH	114988.8	114988.8
	H ₂ O	438114.56	350491.65
peak #	Element	Area	Mole
1	H ₂	1458.4	10901.54
	CO		15426.9
2	CH ₄	6.3	93.87
3	H ₂	3296.6	9438.1658
4	H ₂ O +CO	478516.3	
5	CH ₂ O	1662.1	9806.39
6	C ₂ H ₅ OH	105090	105090
	H ₂ O	477971.18	382376.94
T= 500 C			
peak #	Element	Area	Mole
1	H ₂	2022.1	15115.198
	CO		13734.6
2	CH ₄	75	1117.5
3	H ₂	4839.4	13855.202
4	CO ₂	3.86	25.09
5	CH ₄	99.5	579.09
6	H ₂ O +CO	391676.3	
7	CH ₂ O	1848.4	10905.56
8	C ₂ H ₅ OH	82245.2	82245.2
	H ₂ O	391190.98	312952.78
T= 525 C			
peak #	Element	Area	Mole
1	H ₂	3376.9	25242.328
	CO		24506.55
2	CH ₄	288.7	4301.63
3	H ₂	8026.7	22980.442
4	CO ₂	11	71.5
5	CH ₄	232.8	1354.896

Table 13.(Cont.d)

6	H ₂ O +CO	390314.3	
7	CH ₂ O	2540.4	14988.36
8	C ₂ H ₅ OH	68742.1	68742.1
	H ₂ O	389448.34	311558.68
peak #	Element	Area	Mole
1	H ₂	2915	21789.625
	CO		16018.5
2	CH ₄	144	2145.6
3	H ₂	7109	20353.067
4	CO ₂	10	65
5	CH ₄	233	1356.06
6	H ₂ O +CO	297758.5	
7	CH ₂ O	2740.2	16167.18
8	C ₂ H ₅ OH	61291.7	61291.7
	H ₂ O	297192.48	237753.98
T= 550 C			
peak #	Element	Area	Mole
1	H ₂	5630.3	42086.493
	CO		36564.9
2	CH ₄	313.5	4671.15
3	H ₂	13533.6	38746.697
4	CO ₂	26.7	173.55
5	CH ₄	546.6	3181.212
6	H ₂ O +CO	400282.6	
7	CH ₂ O	1866.6	11012.94
8	C ₂ H ₅ OH	77377.3	77377.3
	H ₂ O	398990.55	319192.44

Table 14. Raw Data Of Ni-HT (I)b

Ni-HT (I)b			
T=350 C			
peak #	Element	Area	Mole
1.0	H ₂	64.9	485.1
	CO		116.6
2.0	H ₂	166.7	477.3
3.0	H ₂ O +CO	643098.0	-
4.0	C ₂ H ₅ OH	176295.0	176295.0
	H ₂ O	643093.9	514475.1
peak #	Element	Area	Mole
1.0	H ₂	53.7	401.4
	CO		522.0
2.0	H ₂	123.0	352.1
3.0	H ₂ O +CO	508778.0	-
4.0	C ₂ H ₅ OH	165929.9	165929.9
	H ₂ O	508759.6	407007.6
T=400 C			
peak #	Element	Area	Mole
1.0	H ₂	266.6	1992.8
	CO		1592.6
2.0	H ₂	645.7	1848.6
3.0	CH ₄	263.7	1534.7
4.0	C ₂ H ₄	97.3	1050.8
5.0	H ₂ O +CO	546362.4	
6.0	CH ₂ O	630.6	3720.5
7.0	C ₂ H ₅ OH	164137.3	180551.0
	H ₂ O	546306.1	437044.9
T= 425 C			
peak #	Element	Area	Mole
1.0	H ₂	538.8	4027.5
	CO		795.0
2.0	CH ₄	9.1	135.1
3.0	H ₂	1390.0	3979.6
4.0	CH ₄	274.5	1597.6
5.0	C ₂ H ₄	22.8	246.2

Table 14 (Cont.d)

6.0	H ₂ O +CO	541372.1	
7.0	CH ₂ O	1247.6	7360.8
8.0	C ₂ H ₅ OH	151793.0	151793.0
	H ₂ O	541344.0	433075.2
T=450 C			
peak #	Element	Area	Mole
1.0	H ₂	916.8	6853.1
	CO		5333.2
2.0	CH ₄	19.4	289.1
3.0	H ₂	2225.5	6371.6
4.0	CH ₄	282.0	1641.2
5.0	C ₂ H ₄	47.9	517.3
6.0	H ₂ O +CO	467836.1	
7.0	CH ₂ O	2105.9	12424.8
8.0	C ₂ H ₅ OH	111858.7	111858.7
	H ₂ O	467647.6	374118.1
T=475 C			
peak #	Element	Area	Mole
1.0	H ₂	1685.8	12601.4
	CO		19178.1
2.0	CH ₄	20.8	309.9
3.0	H ₂	3763.4	10774.6
4.0	H ₂ O +CO	466766.1	
5.0	CH ₂ O	1926.2	11364.6
6.0	C ₂ H ₅ OH	115448.2	115448.2
	H ₂ O	466088.4	372870.7
peak #	Element	Area	Mole
1.0	H ₂	1608.7	12025.0
	CO		14592.6
2.0	CH ₄	10.0	149.0
3.0	H ₂	3721.4	10654.4
4.0	C ₂ H ₄	26.4	285.1
5.0	H ₂ O +CO	438630.2	
6.0	CH ₂ O	2036.6	12015.9
7.0	C ₂ H ₅ OH	114988.8	114988.8

Table 14 (Cont.d)

	H ₂ O	438114.6	350491.6
peak #	Element	Area	Mole
1.0	H ₂	1458.4	10901.5
	CO		15426.9
2.0	CH ₄	6.3	93.9
3.0	H ₂	3296.6	9438.2
4.0	H ₂ O +CO	478516.3	
5.0	CH ₂ O	1662.1	9806.4
6.0	C ₂ H ₅ OH	105090.0	105090.0
	H ₂ O	477971.2	382376.9
T= 500 C			
peak #	Element	Area	Mole
1.0	H ₂	2022.1	15115.2
	CO		13734.6
2.0	CH ₄	75.0	1117.5
3.0	H ₂	4839.4	13855.2
4.0	CO ₂	3.9	25.1
5.0	CH ₄	99.5	579.1
6.0	H ₂ O +CO	391676.3	
7.0	CH ₂ O	1848.4	10905.6
8.0	C ₂ H ₅ OH	82245.2	82245.2
	H ₂ O	391191.0	312952.8
T= 525 C			
peak #	Element	Area	Mole
1.0	H ₂	3376.9	25242.3
	CO		24506.6
2.0	CH ₄	288.7	4301.6
3.0	H ₂	8026.7	22980.4
4.0	CO ₂	11.0	71.5
5.0	CH ₄	232.8	1354.9
6.0	H ₂ O +CO	390314.3	
7.0	CH ₂ O	2540.4	14988.4
8.0	C ₂ H ₅ OH	68742.1	68742.1
	H ₂ O	389448.3	311558.7
peak #	Element	Area	Mole

Table 14 (Cont.d)

1.0	H ₂	2915.0	21789.6
	CO		16018.5
2.0	CH ₄	144.0	2145.6
3.0	H ₂	7109.0	20353.1
4.0	CO ₂	10.0	65.0
5.0	CH ₄	233.0	1356.1
6.0	H ₂ O +CO	297758.5	
7.0	CH ₂ O	2740.2	16167.2
8.0	C ₂ H ₅ OH	61291.7	61291.7
	H ₂ O	297192.5	237754.0
T= 550 C			
peak #	Element	Area	Mole
1.0	H ₂	5630.3	42086.5
	CO		36564.9
2.0	CH ₄	313.5	4671.2
3.0	H ₂	13533.6	38746.7
4.0	CO ₂	26.7	173.6
5.0	CH ₄	546.6	3181.2
6.0	H ₂ O +CO	400282.6	
7.0	CH ₂ O	1866.6	11012.9
8.0	C ₂ H ₅ OH	77377.3	77377.3
	H ₂ O	398990.6	319192.4

Table 15. Raw Data Of Ni-HT (II)

Ni-HT (II)			
T=300			
peak #	element	area	mole
1.0	H ₂	2.0	1748.1
2.0	CO	31.4	1033.1
3.0	CH ₄	14.6	642.4
4.0	CO ₂	5.3	62.8
5.0	H ₂ O	185246.3	257492.4
6.0	CH ₂ O	939.0	1591.6
7.0	C ₂ H ₅ OH	666882.0	666882.0
peak #	element	area	mole
1.0	H ₂	1.9	1660.7
2.0	CO	31.3	1029.8
3.0	CH ₄	15.8	695.2
4.0	CO ₂	4.9	58.1
5.0	H ₂ O	191721.6	266493.0
6.0	CH ₂ O	1110.6	1882.5
7.0	C ₂ H ₅ OH	90844.3	90844.3
peak #	element	area	mole
1.0	H ₂	1.8	1573.3
2.0	CO	34.9	1148.2
3.0	CH ₄	16.9	743.6
4.0	CO ₂	5.3	62.8
5.0	H ₂ O	235267.9	327022.4
6.0	CH ₂ O	1488.8	2523.5
7.0	C ₂ H ₅ OH	103543.6	103543.6
T=350			
peak #	element	area	mole
1.0	H ₂	8.6	7516.8
2.0	CO	300.5	9886.2
3.0	CH ₄	169.2	7444.8
4.0	CO ₂	20.6	244.1
5.0	H ₂ O	131925.0	183375.8
6.0	CH ₂ O	2022.6	3428.3
7.0	C ₂ H ₅ OH	70318.5	70318.5

Table 15 (Cont.d)

peak #	element	area	mole
1.0	H ₂	8.8	7691.6
2.0	CO	346.4	11396.6
3.0	CH ₄	197.5	8690.0
4.0	CO ₂	22.0	260.7
5.0	H ₂ O	127335.0	176995.7
6.0	CH ₂ O	1641.3	2782.0
7.0	C ₂ H ₅ OH	53587.6	53587.6
peak #	element	area	mole
1.0	H ₂	8.3	7254.6
2.0	CO	343.1	11288.0
3.0	CH ₄	196.3	8637.2
4.0	CO ₂	22.8	270.2
5.0	H ₂ O	399851.0	555792.9
6.0	CH ₂ O	2641.1	4476.7
7.0	C ₂ H ₅ OH	65085.2	65085.2
T=400			
peak #	element	area	mole
1.0	H ₂	26.0	22725.3
2.0	CO	1113.6	36635.8
3.0	CH ₄	635.1	27944.4
4.0	CO ₂	126.0	1493.1
5.0	C ₂ H ₄	5.0	500.0
6.0	H ₂ O	163967.9	227915.4
7.0	CH ₂ O	1100.4	1865.1
8.0	C ₂ H ₅ OH	32176.5	32176.5
peak #	element	area	mole
1.0	H ₂	27.5	24036.4
2.0	CO	1178.4	38769.4
3.0	CH ₄	681.4	29981.6
4.0	CO ₂	139.5	1653.1
5.0	C ₂ H ₄	5.8	580.0
6.0	H ₂ O	120919.1	168077.5
7.0	CH ₂ O	942.5	1597.5
8.0	C ₂ H ₅ OH	30990.0	30990.0

Table 15 (Cont.d)

peak #	element	area	mole
1.0	H ₂	25.3	22113.5
2.0	CO	1146.3	37713.3
3.0	CH ₄	662.1	29132.4
4.0	CO ₂	126.7	1501.4
5.0	C ₂ H ₄	5.3	530.0
6.0	H ₂ O	252827.4	351430.1
7.0	CH ₂ O	654.1	1108.7
8.0	C ₂ H ₅ OH	31617.2	31617.2
T=450			
peak #	element	area	mole
1.0	H ₂	52.2	45625.4
2.0	CO	1489.0	48988.1
3.0	CH ₄	921.3	40537.2
4.0	CO ₂	603.2	7147.9
5.0	C ₂ H ₄	5.0	500.0
6.0	H ₂ O	224864.8	312562.1
7.0	CH ₂ O	207.0	350.9
8.0	C ₂ H ₅ OH	5400.3	5400.3
peak #	element	area	mole
1.0	H ₂	46.6	40730.7
2.0	CO	1501.9	49412.5
3.0	CH ₄	861.5	37906.0
4.0	CO ₂	486.1	5760.3
5.0	C ₂ H ₄	5.0	500.0
6.0	H ₂ O	123129.2	171149.6
7.0	CH ₂ O	243.8	413.2
8.0	C ₂ H ₅ OH	7975.3	7975.3
peak #	element	area	mole
1.0	H ₂	59.5	52006.0
2.0	CO	1318.6	43381.9
3.0	CH ₄	900.3	39613.2
4.0	CO ₂	918.9	10889.0
5.0	C ₂ H ₄	5.0	500.0
6.0	H ₂ O	86293.6	119948.1

Table 15 (Cont.d)

7.0	CH ₂ O	712.2	1207.2
8.0	C ₂ H ₅ OH	5784.6	5784.6
T=500			
peak #	element	area	mole
1.0	H ₂	69.8	61008.7
2.0	CO	1189.2	39124.7
3.0	CH ₄	616.2	27112.8
4.0	CO ₂	1105.0	13094.3
5.0	C ₂ H ₄	7.6	760.0
6.0	H ₂ O	494470.9	687314.6
7.0	CH ₂ O	445.9	755.8
8.0	C ₂ H ₅ OH	2065.8	2065.8
peak #	element	area	mole
1.0	H ₂	84.2	73595.0
2.0	CO	1245.2	40967.1
3.0	CH ₄	607.1	26712.4
4.0	CO ₂	1297.4	15374.2
5.0	C ₂ H ₄	7.6	760.0
6.0	H ₂ O	86662.0	120460.2
7.0	CH ₂ O	981.4	1663.5
8.0	C ₂ H ₅ OH	5994.5	5994.5
peak #	element	area	mole
1.0	H ₂	59.8	52268.2
2.0	CO	917.9	30198.9
3.0	CH ₄	406.2	17872.8
4.0	CO ₂	998.9	11837.0
5.0	C ₂ H ₄	7.0	700.0
6.0	H ₂ O	130744.2	181734.4
7.0	CH ₂ O	1269.1	2151.1
8.0	C ₂ H ₅ OH	9610.9	9610.9
T=550			
peak #	element	area	mole
1.0	H ₂	108.8	95096.6
2.0	CO	1210.5	39825.5
3.0	CH ₄	429.7	18906.8

Table 15 (Cont.d)

4.0	CO ₂	1802.4	21358.4
5.0	C ₂ H ₄	7.8	780.0
6.0	H ₂ O	88421.8	122906.3
7.0	CH ₂ O	498.3	844.6
8.0	C ₂ H ₅ OH	5985.5	5985.5
peak #	element	area	mole
1.0	H ₂	98.9	86443.5
2.0	CO	1135.5	37358.0
3.0	CH ₄	379.3	16689.2
4.0	CO ₂	1694.3	20077.5
5.0	C ₂ H ₄	9.2	920.0
6.0	H ₂ O	174175.0	242103.3
7.0	CH ₂ O	583.5	989.0
8.0	C ₂ H ₅ OH	8278.5	8278.5
peak #	element	area	mole
1.0	H ₂	103.1	90114.6
2.0	CO	1124.1	36982.9
3.0	CH ₄	380.0	16720.0
4.0	CO ₂	1762.4	20884.4
5.0	C ₂ H ₄	10.0	1000.0
6.0	H ₂ O	14106.0	19607.3
7.0	CH ₂ O	132.4	224.4
8.0	C ₂ H ₅ OH	615.5	615.5

Table 16. Raw Data Of Cu-HT (I)

Cu-HT (I)			
T=300			
peak #	element	area	mole
1	C ₂ H ₄	131.1	13110
2	H ₂ O	136318	189482.02
3	C ₂ H ₅ OH	59459	59459
peak #	element	area	mole
1	C ₂ H ₄	355	35500
2	H ₂ O	213703	297047.17
3	C ₂ H ₅ OH	62177.6	62177.6
peak #	element	area	mole
1	C ₂ H ₄	254	25400
2	H ₂ O	133217	185171.63
3	C ₂ H ₅ OH	64599.5	64599.5
T=350			
peak #	element	area	mole
1	H ₂	1	874
2	CO	1	32.9
3	CH ₄	1	44
4	CO ₂	1	11.85
5	C ₂ H ₄	299.4	29940
6	H ₂ O	133707	185852.73
7	CH ₂ O	628.365	1065.0787
8	C ₂ H ₅ OH	48498.5	48498.5
peak #	element	area	mole
1	H ₂	1	874
2	CO	1.1	36.19
3	CH ₄	1	44
4	CO ₂	1	11.85
5	C ₂ H ₄	323.9	32390
6	H ₂ O	201011	279405.29
7	CH ₂ O	834	1413.63
8	C ₂ H ₅ OH	71044	71044
T=400			
peak #	element	area	mole

Table 16 (Cont.d)

1	H ₂	1.7	1485.8
2	CO	1.7	55.93
3	CH ₄	1.1	48.4
4	CO ₂	1.1	13.035
5	C ₂ H ₄	293.2	29320
6	H ₂ O	140419.6	195183.24
7	CH ₂ O	1289.9	2186.3805
8	C ₂ H ₅ OH	60702.9	60702.9
peak #	element	area	mole
1	H ₂	2	1748
2	CO	1.08	35.532
3	CH ₄	1.1	48.4
4	CO ₂	1	11.85
5	C ₂ H ₄	299.5	29950
6	H ₂ O	147276	204713.64
7	CH ₂ O	714.8	1211.586
8	C ₂ H ₅ OH	56069.7	56069.7
peak #	element	area	mole
1	H ₂	1.4	1223.6
2	CO	1.31	43.099
3	CH ₄	1.1	48.4
4	CO ₂	1.1	13.035
5	C ₂ H ₄	521	52100
6	H ₂ O	127270	176905.3
7	CH ₂ O	794.8	1347.186
8	C ₂ H ₅ OH	73549.6	73549.6
T=450			
peak #	element	area	mole
1	H ₂	2	1748
2	CO	3.16	103.964
3	CH ₄	1.1	48.4
4	CO ₂	1.1	13.035
5	C ₂ H ₄	32.4	3240
6	H ₂ O	145265	201918.35
7	CH ₂ O	1164.7	1974.1665

Table 16 (Cont.d)

8	C ₂ H ₅ OH	85432.7	85432.7
peak #	element	area	mole
1	H ₂	1.4	1223.6
2	CO	1.58	51.982
3	CH ₄	1.1	48.4
4	CO ₂	2.8	33.18
5	C ₂ H ₄	40.5	4050
6	H ₂ O	136251.4	189389.45
7	CH ₂ O	1244	2108.58
8	C ₂ H ₅ OH	73995.6	73995.6
peak #	element	area	mole
1	H ₂	1.04	908.96
2	CO	1.4	46.06
3	CH ₄	1	44
4	CO ₂	1.5	17.775
5	C ₂ H ₄	57.3	5730
6	H ₂ O	136437	189647.43
7	CH ₂ O	1209	2049.255
8	C ₂ H ₅ OH	73448.3	73448.3
T=500			
peak #	element	area	mole
1	H ₂	1.26	1101.24
2	CO	4.2	138.18
3	CH ₄	1.85	21.9225
4	CO ₂	1	44
5	C ₂ H ₄	146.2	14620
6	H ₂ O	126673	176075.47
7	CH ₂ O	1084.9	1838.9055
8	C ₂ H ₅ OH	44274	44274
peak #	element	area	mole
1	H ₂	1.2	1048.8
2	CO	3.3	108.57
3	CH ₄	1.1	48.4
4	CO ₂	3.1	36.735
5	C ₂ H ₄	99.2	9920

Table 16 (Cont.d)

6	H ₂ O	470009	653312.51
7	CH ₂ O	1635.5	2772.1725
8	C ₂ H ₅ OH	84546.4	84546.4
peak #	element	area	mole
1	H ₂	1.5	1311
2	CO	3.8	125.02
3	CH ₄	1.01	44.44
4	CO ₂	3.6	42.66
5	C ₂ H ₄	112.2	11220
6	H ₂ O	136443	189655.77
7	CH ₂ O	1030	1745.85
8	C ₂ H ₅ OH	60131.6	60131.6
T=550			
peak #	element	area	mole
1	H ₂	3.8	3321.2
2	CO	7.9	259.91
3	CH ₄	3.8	167.2
4	CO ₂	6	71.1
5	C ₂ H ₄	399.9	39990
6	H ₂ O	214095	297592.05
7	CH ₂ O	2282.8	3869.346
8	C ₂ H ₅ OH	91239	91239
peak #	element	area	mole
1	H ₂	2.4	2097.6
2	CO	3.8	125.02
3	CH ₄	2.1	24.885
4	CO ₂	4.7	55.695
5	C ₂ H ₄	363.9	36390
6	H ₂ O	128861.7	179117.76
7	CH ₂ O	1491.9	2528.7705
8	C ₂ H ₅ OH	38471.1	38471.1
peak #	element	area	mole
1	H ₂	2.1	1835.4
2	CO	3.3	108.57
3	CH ₄	1.54	18.249

Table 16 (Cont.d)

4	CO ₂	3.05	36.1425
5	C ₂ H ₄	345	34500
6	H ₂ O	125480	174417.2
7	CH ₂ O	1443	2445.885
8	C ₂ H ₅ OH	33214.2	33214.2

Table 17. Raw Data Of Cu-Imp (II)

Cu-Imp (II)			
T=300C			
peak #	element	Area	mole
1	H ₂	3.3	2884.365
2	CO	1	32.9
3	CO ₂	1	11.85
4	CH ₄	0.7	30.8
5	H ₂ O	102909.2	143043.79
6	CH ₂ O	1995.8	3382.881
7	C ₂ H ₅ OH	26620.1	26620.1
peak #	element	Area	mole
1	H ₂	5.33	4658.6865
2	CO	1	32.9
3	CO ₂	1	11.85
4	CH ₄	0.88	38.72
5	H ₂ O	371941.1	516998.13
6	CH ₂ O	4768.4	8082.438
7	C ₂ H ₅ OH	127789.6	127789.6
T=350			
peak #	element	Area	mole
1	H ₂	11.05	9658.2525
2	CO	1.7	55.93
3	CO ₂	31	367.35
4	C ₂ H ₄	28.4	2840
5	CH ₄	2.7	118.8

Table 17 (Cont.d)

6	H ₂ O	134121	186428.19
7	CH ₂ O	5321.6	9020.112
8	C ₂ H ₅ OH	36913.6	36913.6
peak #	element	Area	mole
1	H ₂	8.4	7342.02
2	CO	1.7	55.93
3	CO ₂	1	11.85
4	C ₂ H ₄	29.7	2970
5	CH ₄	1.2	52.8
6	H ₂ O	171450	238315.5
7	CH ₂ O	5272.7	8937.2265
8	C ₂ H ₅ OH	65875	65875
peak #	element	Area	mole
1	H ₂	5	4370.25
2	CO	1.3	42.77
3	CO ₂	1	11.85
4	CH ₄	1.14	50.16
5	C ₂ H ₄	33.2	3320
6	H ₂ O	123264	171336.96
7	CH ₂ O	3311	5612.145
8	C ₂ H ₅ OH	46329	46329
T=400			
peak #	element	Area	mole
1	H ₂	3.77	3295.1685
2	CO	1.09	35.861
3	CO ₂	1.5	17.775
4	CH ₄	1.1	48.4
5	C ₂ H ₄	126.1	12610
6	H ₂ O	346159.8	481162.12
7	CH ₂ O	2109.2	3575.094
8	C ₂ H ₅ OH	64439.1	64439.1
peak #	element	Area	mole
1	H ₂	4.18	3653.529
2	CO	1.1	36.19
3	CO ₂	1.7	20.145

Table 17 (Cont.d)

4	CH ₄	1.1	48.4
5	C ₂ H ₄	133.8	13380
6	H ₂ O	428451	595546.89
7	CH ₂ O	3378.1	5725.8795
8	C ₂ H ₅ OH	124425.7	124425.7
T=450			
peak #	element	Area	mole
1	H ₂	4.5	3933.225
2	CO	2.9	95.41
3	CO ₂	2.48	29.388
4	CH ₄	1.87	82.28
5	C ₂ H ₄	414	41400
6	H ₂ O	156780	217924.2
7	CH ₂ O	1968.1	3335.9295
8	C ₂ H ₅ OH	37996	37996
peak #	element	Area	mole
1	H ₂	3.8	3321.39
2	CO	2.54	83.566
3	CO ₂	2.79	33.0615
4	CH ₄	1.7	74.8
5	C ₂ H ₄	411.6	41160
6	H ₂ O	488590	679140.1
7	CH ₂ O	2668.5	4523.1075
8	C ₂ H ₅ OH	74976.9	74976.9
T=500			
peak #	element	Area	mole
1	H ₂	2.9	2534.745
2	CO	7.2	236.88
3	CH ₄	5.4	237.6
4	CO ₂	8.5	100.725
5	C ₂ H ₄	1030	103000
6	H ₂ O	522977	726938.03
7	CH ₂ O	1897.9	3216.9405
8	C ₂ H ₅ OH	42954	42954
peak #	element	Area	mole

Table 17 (Cont.d)

1	H ₂	2.1	1835.505
2	CO	6.7	220.43
3	CH ₄	5.2	228.8
4	CO ₂	8.8	104.28
5	C ₂ H ₄	1004.5	100450
6	H ₂ O	212411.1	295251.43
7	CH ₂ O	820.9	1391.4255
8	C ₂ H ₅ OH	33360	33360
T=550			
peak #	element	Area	mole
1	H ₂	2.6	2272.53
2	CO	14.534	478.1686
3	CH ₄	9.3	409.2
4	CO ₂	11.3	133.905
5	C ₂ H ₄	1476	147600
6	H ₂ O	332390	462022.1
7	CH ₂ O	1421.6	2409.612
8	C ₂ H ₅ OH	22736.4	22736.4
peak #	element	Area	mole
1	H ₂	2	1748.1
2	CO	11	361.9
3	CH ₄	6.6	290.4
4	CO ₂	11.8	139.83
5	C ₂ H ₄	1209	120900
6	H ₂ O	7.139	9.92321
7	CH ₂ O	1160.6	1967.217
8	C ₂ H ₅ OH	30788.9	30788.9

APPENDIX B.2. CALIBRATION FACTORS (BETA FACTORS)
OF THE SPECIES

The beta factor of an element was obtained by using Eqn. B.2..

$$\frac{x_A}{x_{C_2H_5OH}} = \frac{Area_A \times \beta_A}{Area_{C_2H_5OH} \times \beta_{C_2H_5OH}} \quad (B.2)$$

The beta factors obtained by plugging the calibration areas ($Area_A$) and fraction of the elements (x_A) as the Ni-HT (I) were analyzed by CTR column are tabulated in Table 18.

Table 18 The calibration values for elements using CTR column

Element	# of peaks	For Ni-HT (I) sample (CTR column)			
		β_1	β_2	Location of peak 1	Location of peak 2
H ₂	2	7.48	2.86	2.6-2.7	5.2-5.3
CO	1	75	-	15.6-15.7	-
CH ₄	2	14.9	5.82	4.3-4.4	14.2-14.6
CO ₂	1	6.5	-	8.2-8.3	-
C ₂ H ₄	1	10.8	-	9.8-9.9	
CH ₂ O	1	3.36	-	26.7-27	-
H ₂ O	1	0.8	-	15.7-16	-
C ₂ H ₅ OH	1	1	-	28.8-29.1	-

The beta factors obtained by plugging the calibration areas ($Area_A$) and fraction of the elements (x_A) as the Ni-HT (II), Cu-HT (I) and Cu-Imp (II) were analyzed by CTR column are tabulated in Table 19

Table 19 The calibration values for elements using Porapak S column

Element	For Ni-HT (II), Cu-HT (I) and Cu-Imp (II) sample (Porapak S column)	
	β_1	Location of the peak
H ₂	874.05	0.264-0.266
CO	32.9	0.331-0.333
CH ₄	44	0.485-0.488
CO ₂	11.85	1.178-1.199
C ₂ H ₄	100	2-2.05
CH ₂ O	1.70	8.354
H ₂ O	1.39	7.039-7.1
C ₂ H ₅ OH	1	9.8-9.9

APPENDIX B.3. SAMPLE CALCULATIONS OF THE REACTION PARAMETERS

The raw data of Ni-HT (II) sample at 550°C is given in Table 20 below.

Table 20. Raw Data of Ni-HT (II) at 550°C

Element	Area	Location
H ₂	103.1	0.264
CO	1124.1	0.331
CH ₄	380	0.485
CO ₂	1762.4	1.178
C ₂ H ₄	10	2.052
H ₂ O	14106	7.039
CH ₂ O	132.4	8.354
C ₂ H ₅ OH	615.5	9.939

$$\text{Mole of element } A = \text{Area}_A \times \beta_A \quad (\text{A.2.1})$$

$$\text{Mole of element } H_2 = (H_2)_{out} = 103.1 \times 874.05 \rightarrow 90114.56 \text{ moles}$$

$$\text{Mole of element } CO = (CO)_{out} = 1124.1 \times 32.9 \rightarrow 36982.89 \text{ moles}$$

$$\text{Mole of element } CH_4 = (CH_4)_{out} = 380 \times 44 \rightarrow 16720 \text{ moles}$$

$$\text{Mole of element } CO_2 = (CO_2)_{out} = 1762.4 \times 11.85 \rightarrow 20884.44 \text{ moles}$$

$$\text{Mole of element } C_2H_4 = (C_2H_4)_{out} = 10 \times 100 \rightarrow 1000 \text{ moles}$$

$$\text{Mole of element } H_2O = (H_2O)_{out} = 14106 \times 1.39 \rightarrow 19607.34 \text{ moles}$$

$$\text{Mole of element } CH_2O = (CH_2O)_{out} = 132.4 \times 1.70 \rightarrow 224.42 \text{ moles}$$

$$\text{Mole of element } C_2H_5OH = (C_2H_5OH)_{out} = 615.5 \times 1 \rightarrow 615.5 \text{ moles}$$

Carbon Balance;

$$C_{2m} = (C_2H_5OH)_{in} = \frac{(CO)_{out}}{2} + \frac{(CH_4)_{out}}{2} + \frac{(CO_2)_{out}}{2} + (C_2H_4)_{out} + \frac{(CH_2O)_{out}}{2} + (C_2H_5OH)_{out}$$

$$C_{2m} = (C_2H_5OH)_{in} = \frac{3698289}{2} + \frac{16720}{2} + \frac{2088444}{2} + 1000 + \frac{22442}{2} + 615.5 \rightarrow 3902137 \text{ moles}$$

EtOH Conversion was calculated from Eqn.(4) given in Section 5.2.i.

$$X_{C_2H_5OH} = \frac{\text{Moles of } C_2H_5OH \text{ converted}}{\text{Moles of } C_2H_5OH \text{ fed to the reactor}} \quad (4)$$

$$X_{C_2H_5OH} = \frac{39021.37 - 615.5}{39021.37} \rightarrow 0.98$$

Yield of Hydrogen was calculated from Eqn. (5) given in Section 5.2.ii.

$$Y_{H_2} = \frac{\text{Moles of } H_2 \text{ produced}}{\text{Moles of } C_2H_5OH \text{ fed to the reactor}} \quad (5)$$

$$Y_{H_2} = \frac{90114.56}{39021.37} \rightarrow 2.31$$

Selectivity of Side Products were calculated from Eqn. (6)

$$(\text{Selectivity of product A}) S_A = \frac{\text{Moles of A formed}}{\text{Moles of } C_2H_5OH \text{ converted}} \quad (6)$$

$$S_{CO} = \frac{36982.89}{39021.37 - 615.5} \rightarrow 0.96$$

$$S_{CH_4} = \frac{16720}{39021.37 - 615.5} \rightarrow 0.44$$

$$S_{CO_2} = \frac{20884.44}{39021.37 - 615.5} \rightarrow 0.54$$

$$S_{C_2H_4} = \frac{1000}{39021.37 - 615.5} \rightarrow 0.03$$

$$S_{CH_2O} = \frac{224.42}{39021.37 - 615.5} \rightarrow 0.006$$

Table 21. Calculated Reaction Parameters

Ni-HT (Ia)							
<i>Temp</i>	$X_{C_2H_5OH}$	S_{CO}	S_{CH_4}	S_{CO_2}	S_{CH_2O}	$S_{C_2H_4}$	<i>Yield of H₂</i>
400	0.04	0.21	0.03	0	0.49	0.19	0.02
425	0.03	0.08	0.01	0	0.72	0.05	0.03
450	0.08	0.26	0.01	0	0.61	0.05	0.05
475	0.11	0.54	0.005	0	0.44	0.02	0.08
500	0.13	0.54	0.02	0.001	0.43	0	0.15
525	0.23	0.52	0.03	0.002	0.41	0	0.26
550	0.36	0.42	0.04	0.002	0.13	0	0.32
Ni-HT (Ib)							
<i>Temp</i>	$X_{C_2H_5OH}$	S_{CO}	S_{CH_4}	S_{CO_2}	S_{CH_2O}	$S_{C_2H_4}$	<i>Yield of H₂</i>
400	0.06	0.09	0	0	0.91	0.002	0.02
425	0.17	0.43	0.04	0	0.53	0.003	0.14
450	0.29	0.53	0.1	0	0.38	0	0.33
475	0.56	0.68	0.18	0.003	0.26	0	0.88
500	0.92	0.64	0.32	0.005	0.03	0	1.64
525	1	0.65	0.34	0.01	0	0	1.49

Table 21. Calculated Reaction Parameters (Cont.d)

Ni-HT (II)							
<i>Temp</i>	$X_{C_2H_5OH}$	S_{CO}	S_{CH_4}	S_{CO_2}	S_{CH_2O}	$S_{C_2H_4}$	<i>Yield of H₂</i>
300	0.01	0.57	0.37	0.03	1.04	-	0.01
350	0.16	0.95	0.72	0.02	0.31	-	0.10
400	0.53	1.06	0.82	0.04	0.04	0.02	0.34
450	0.88	0.98	0.82	0.16	0.01	0.01	0.85
500	0.87	0.95	0.62	0.35	0.04	0.05	1.40
550	0.89	0.97	0.44	0.53	0.02	0.05	2.06
Cu-HT (I)							
<i>Temp</i>	$X_{C_2H_5OH}$	S_{CO}	S_{CH_4}	S_{CO_2}	S_{CH_2O}	$S_{C_2H_4}$	<i>Yield of H₂</i>
300	0.28	0	0	0	0	1.00	0.00
350	0.35	0.001	0.001	0	0.04	0.98	0.01
400	0.37	0.001	0.001	0	0.05	0.98	0.02
450	0.07	0.01	0.009	0	0.39	0.79	0.02
500	0.18	0.01	0.004	0.003	0.17	0.91	0.02
550	0.44	0.004	0.002	0.001	0.08	0.96	0.03

Table 21. Calculated Reaction Parameters (Cont.d)

Cu-Imp (II)							
<i>Temp</i>	$X_{C_2H_5OH}$	S_{CO}	S_{CH_4}	S_{CO_2}	S_{CH_2O}	$S_{C_2H_4}$	<i>Yield of H₂</i>
300	0.05	0.013	0.013	0.098	1.88	0	0.07
350	0.13	0.007	0.010	0.017	1.09	0.44	0.13
400	0.15	0.002	0.003	0.001	0.30	0.85	0.03
450	0.48	0.002	0.002	0.003	0.09	0.95	0.04
500	0.73	0.002	0.002	0.001	0.02	0.99	0.02
550	0.83	0.003	0.003	0.001	0.02	0.99	0.01